Journal of Hydrology 668 (2026) 135003

Contents lists available at ScienceDirect

Journal of Hydrology

journal homepage: www.elsevier.com/locate/jhydrol

Research papers

Impact of changing recharge on a sole-source coastal aquifer: multi-model assessment for Virginia's Eastern Shore

Farshad Hesamfar [a,*,1], Sergio A. Barbosa [b,c,1], Thanh-Nhan-Duc Tran [a], Teresa Culver [a], Lawrence Band [a], Venkataraman Lakshmi [a]

[a] Dept. of Civil and Environmental Engineering, University of Virginia, Charlottesville, VA 22904, USA
[b] Environmental Institute, University of Virginia, Charlottesville, VA 22904, USA
[c] Environmental Sciences Division, Oak Ridge National Laboratory, Oak Ridge, TN 37831, USA

ARTICLE INFO

This manuscript was handled by Renato Morbidelli, Editor-in-Chief, with the assistance of Mohsen Sherif, Associate Editor

Keywords:
Coastal aquifers
Recharge variability
Scenario-based modeling
CMIP6
Groundwater security
Eastern Shore of Virginia

ABSTRACT

Coastal aquifers face compound pressures from shifting meteorological patterns and sea-level rise (SLR), posing a direct threat to groundwater resources. We estimate future climate-driven recharge by forcing SWAT with downscaled, bias-corrected CMIP6 climate projections from four General Circulation Models (MIROC6, BCC-CSM2-MR, CanESM5, and MRI-ESM2-0) under SSP2-4.5 and SSP5-8.5. These recharge rates, in addition to local SLR, are input into SEAWAT, a variable-density groundwater flow and solute-transport model. Simulations then project changes in the coastal aquifer system over the Eastern Shore of Virginia (ESVA), quantifying groundwater availability and salinity risk from 2023 to 2080. Our findings are: (1) by 2080, the driest scenario (BCC-CSM2-MR; SSP2-4.5) reduces inland surficial groundwater heads by more than one meter and decreases freshwater volume by approximately 100 million m^3 (−2.5%), an amount equivalent to 4.8 yrs of the current total water demand on ESVA. (2) The wettest scenario (CanESM5; SSP2-4.5) increases groundwater heads up to 1.9 m and expands freshwater volume by +2.7%, corresponding to 17 yrs of residential water supply. (3) While the equal-weight ensemble median head change remains small ($|\text{median } \Delta h| \lesssim 5$ cm), the inter-model variability in freshwater storage, measured by the interquartile range (IQR), increases from ~25 MCM in 2030 to ~46 MCM in 2060, indicating growing uncertainty. (4) Groundwater head variation peaks along the central upland ridge (>2 m) but drops below 0.25 m on barrier islands, where sea-level rise dominates. (5) High-emission scenarios show greater groundwater variability before 2060 but converge afterward, while intermediate scenarios show the opposite trend. These findings indicate the need for developing adaptive, climate-resilient groundwater management strategies to enhance water security and mitigate saltwater intrusion.

Abbreviations: CMIP-x, Coupled Model Intercomparison Project, phase x (e.g., CMIP-5, CMIP-6); ΔP/ΔT, Change in precipitation/temperature extracted from a GCM; ET, Evapotranspiration; GCM, General Circulation Models or sometimes Global Climate Models; GHG, Greenhouse Gas; CGCM1, Canadian Global Coupled Climate Model, version 1; SRES, IPCC's Special Report on Emissions Scenarios; GW, Groundwater; GHB, General-Head Boundary in MODFLOW/SEAWAT; GHM, Global Hydrological Model; GPM, Global Precipitation Measurement; HELP, Hydrological Evaluation of Landfill Performance code (water-balance module); IMERG, Integrated Multi-satellitE Retrievals for GPM, a NASA Satellite rainfall product; MODFLOW, USGS MODular Finite-Difference Ground-Water-FLOW model; MODPATH, Particle-tracking post-processor for MODFLOW; RCP x.y, Representative Concentration Pathway with radiative forcing x.y W m^{-2} in 2100 (CMIP-5); RCM, Regional Climate Model (e.g., EURO-CORDEX); SEAWAT, USGS code that couples MODFLOW (flow) & MT3DMS (transport) for variable-density simulations; SLR, Sea-Level Rise; SP/SSP, Shared Socio-economic Pathway (CMIP-6 forcing storyline, e.g., SSP2-4.5); SUTRA, USGS Saturated–Unsaturated TRAnsport model; SVR/SVM, Support-Vector Regression/Machine-Learning Support Vector Machine; SWAT, Soil and Water Assessment Tool (land-surface hydrology model); SWI, Seawater Intrusion; TDS, Total Dissolved Solids.

* Corresponding author.
E-mail addresses: wky7xx@virginia.edu (F. Hesamfar), barbosacassa@ornl.gov (S.A. Barbosa), syu3cs@virginia.edu (T.-N.-D. Tran), tbc4e@virginia.edu (T. Culver), leb3t@virginia.edu (L. Band), vlakshmi@virginia.edu (V. Lakshmi).

[1] These authors contributed equally to this work.

https://doi.org/10.1016/j.jhydrol.2026.135003
Received 10 September 2025; Received in revised form 31 December 2025; Accepted 19 January 2026
Available online 22 January 2026

1. Introduction

Climate change and its variability are reshaping coastal groundwater systems worldwide (Richardson et al. 2024). The impact of climate variability on groundwater resources is a growing concern, as shifts in temperature, precipitation patterns, and extreme weather events influence groundwater availability and recharge (Daoetal.,2024; Davamanietal.,2024; Marshalletal.,2025;Richardsonetal.,2024). These changes can significantly affect aquifer storage and sustainability. Altered recharge rates may exacerbate groundwater depletion and undermine long-term water security and resilience (Asokaetal.,2017; de Graaf et al., 2017; Russo and Lall, 2017; Sivarajanetal.,2019; van der Knaap et al., 2015; van Engelenburgetal.,2017).

Coastal aquifers are especially vulnerable to climate-induced stress due to their distinct hydrogeology and exposure to marine and atmospheric influences, leading to risks like sea-level rise, groundwater depletion, and saltwater intrusion (Polemio 2016; Vespasiano et al. 2019; Herrera-García et al. 2021; Cianflone et al. 2022). In these regions, rising sea levels, changing precipitation regimes, and more frequent extreme weather events may not only reduce freshwater availability (Tran et al. 2023; Vu et al. 2024; Saeedi et al. 2022) but also heighten the risk of saltwater intrusion (Tapas et al. 2024; Ketabchi et al. 2016), complicating groundwater management and planning. This is especially concerning in low-lying coastal areas, where groundwater is often the primary freshwater source (Hesamfaretal.,2023a,b, Tran et al. 2024a). Ensuring the sustainability of these coastal aquifer systems is essential for maintaining long-term regional water security (IGRAC,2024).

*A*pproximately 70% of the world's coastlines are topography-limited, where low-relief topography keeps the water table near the land surface (Michael et al., 2013). In these systems, the water table cannot rise much with sea-level rise, reducing the land-to-sea hydraulic gradient and fresh groundwater flow, and making them more vulnerable to seawater intrusion (Werner and Simmons, 2009; Chang et al., 2011; Werner et al., 2012). Virginia's Eastern Shore (ESVA), a narrow, low-lying peninsula between the Atlantic Ocean and Chesapeake Bay, exemplifies these challenges. The region relies exclusively on a multilayered aquifer system designated as a sole-source aquifer by the U.S. EPA (EPA 2025), supplying all domestic, agricultural, industrial, and ecological needs (VADEQ, 2024). However, SLR and climate variability pose serious threats to the system's reliability (Andrewsetal.,2019). Despite this, limited studies have investigated climate impacts on these multi-layer groundwater dynamics, with most research focused on surface waters and ecosystem health (Chesapeake Bay Foundation 2018; U. S. Fish & Wildlife Service 2018). There are limited previous regional investigations into groundwater–surface water interactions on the ESVA (Nowroozietal.,1999; Sanford and Pope, 2010, 2007), and none have included future changes in both recharge and SLR.

Numerical modeling is a widely adopted tool for assessing the impacts of climate change on coastal aquifers, which are vulnerable to salinization. However, many studies such as (Akhtar et al., 2022; Chun et al., 2018; EL Hamidi et al., 2021; Hagagg, 2018; Sherif and Singh, 1999; Sithara et al., 2020), have primarily focused on the direct impacts, such as sea-level rise, while overlooking important indirect factors such as recharge variability, evapotranspiration, river stage fluctuations, and changing water demand. Although the importance of these complexities is increasingly recognized, existing modeling efforts remain fragmented. Some studies assess recharge in isolation without simulating groundwater system responses (Barnard et al. 2025); others apply coupled models based on a single climate scenario while neglecting SLR (Scibek et al. 2007); and many rely on steady-state assumptions that fail to capture transient hydrological processes (Scibek and Allen 2006). For example, Barnard et al. (2025) projected shallow water-table rise in the southeastern United States using a fixed-recharge, steady-state model that excluded both salinity and recharge variability, whereas Ashofteh et al. (2025) linked climate projections to groundwater levels without accounting for marine boundaries or density-driven flow.

In contrast, (Aladejana et al. 2020; Han and Currell 2022; Lam et al. 2021; Oude Essink et al. 2010; Rahimi et al. 2020; Ranjan et al. 2006; Tam et al. 2016) studies have employed more comprehensive modeling approaches integrating multiple stressors such as land use change, surface–groundwater interactions, and transient recharge, which provide more robust and realistic projections of groundwater dynamics and salinization under future climate scenarios. In fact, in some locations, reductions in recharge were found to have a greater influence on saltwater intrusion than SLR itself (Payne 2010). Additional studies have emphasized the influence of human and environmental factors, such as shifting irrigation demands (Zhou et al. 2010), and the presence of drainage systems (Vandenbohede and Lebbe 2010), in shaping aquifer responses to climate change.

While integrating all major climate stressors is essential for reliable groundwater level and freshwater-storage projections, many existing models rely on simplified 2D frameworks that cannot fully capture the spatial and temporal dynamics of complex coastal aquifer systems (Tiwari et al. 2024). Addressing this, Tiwari et al. (2024) recently developed a 3D variable-density SEAWAT model for the Metaponto aquifer in Italy, incorporating historical and projected conditions, salinity transport, and irrigation demand using a GIS-based inverse water balance approach. However, their study focuses on a relatively small ($\sim$42 km^2), single unconfined aquifer and estimates recharge using simplified methods based on precipitation, evapotranspiration, and infiltration coefficients. Additionally, the climate inputs are based on earlier-generation projections (CMIP3/CMIP5) and literature-derived rainfall decline estimates. Table 1 summarizes the principal modelling approaches, climate forcings, and knowledge gaps identified in prior studies relative to the methods applied in this work.

This research extends the regional groundwater modeling framework developed by Sanford et al. (2009), which represents the heterogeneous hydrostratigraphy and spatial variability of groundwater pumping across the peninsula. While routinely updated by the Virginia Department of Environmental Quality (VADEQ, 2024), the existing model relies on fixed recharge rates and does not account for projected climate or sea-level changes.

To overcome these limitations, the model was enhanced by integrating transient recharge estimates derived from bias-corrected, downscaled CMIP6 GCMs (Thrasher et al., 2022; NEX-GDDP-CMIP6, 2025) through SWAT simulations under both emission scenarios (Tran and Lakshmi 2024). This study presents an open-loop, multi-model scenario ensemble. Sea-level rise projections were incorporated as a time-varying General Head Boundary (GHB) condition based on trends in NOAA tides and currents data (NOAA,2024). Simulations were performed with SEAWAT's coupled variable-density flow and solute transport, in which groundwater density varies with simulated chloride concentration; reported heads are equivalent freshwater heads. The associated density-driven pressure differences are handled internally by SEAWAT through the Variable-Density Flow (VDF) package. This configuration enables evaluation of dynamic hydrologic responses and density-dependent salinization under combined recharge and sea-level forcing.

This study aims to develop an improved transient modeling framework that integrates climate-driven recharge variability to realistically evaluate groundwater levels and salinity responses under future climate scenarios. By integrating high-resolution climate projections with land surface hydrologic modeling and variable-density groundwater flow and solute-transport simulations, this approach advances prior efforts, enhancing the capacity to assess future coastal groundwater conditions. The methodology offers broad applicability to other climate-sensitive coastal aquifers confronting similar challenges.

Table 1
Comparative review of related groundwater–climate studies and the present ESVA analysis.

Reference/model chain	Study setting	Density-dependent flow?	SLR* represented?	How SLR is imposed	Coastal surface processes †	Climate forcing	No. of GCMs*	CMIP* generation & scenarios	Ground-water time-step/stress periods	Temporal resolution of recharge & SLR signal	Distinctive elements claimed by authors	Principal gaps
(Michael et al. 2013) 2D SUTRA model	Global coastline typology (vulnerability study)	×	✓	Analytical 2-D sharp-interface; sea head raise	×	None (parametric)	—	—	Steady-state	N/A	Global first-order typology, classifies coasts as topography- vs recharge-limited	No GCMs, Not site-specific, no transient hydrology
(Scibek et al. 2007; Scibek and Allen 2006) HELP* + MODFLOW	Interior valley aquifer, British Columbia, Canada	×	× (inland site)	—	—	1 CGCM1* (CMIP-2), ΔP & ΔT *	1	SRES* A2/B2	Monthly	Monthly recharge only	Climate impacts via recharge and river flows to GW *	no SLR*, no density, outdated climate model
(Sithara et al. 2020) SEAWAT	Alluvial strip, Kerala coastal strip, India	✓	✓	SEAWAT constant-head cells (GHB*) raised	×	CMIP-5 RCP4.5/8.5* (GCM ensemble via SVM*)	1 – statistical	CMIP-5	Monthly	One-time SLR rise	Machine-learning (SVM) sea-level forecast	Single GCM equivalent; no land recharge coupling; steady-state
(Yang et al. 2023) SWAT–MODFLOW–SEAWAT	Yellow River Delta, Deltaic coast, China	✓	×	—	×	6 CMIP-6 GCMs, SSP1-2.6 & 5–8.5 (precip. only)	6	CMIP-6	Daily SWAT, monthly MODFLOW	Monthly recharge	First fully unified SWAT-MODFLOW-SEAWAT tool; bias-corrected GCMs	No sea-level boundary change; no density coupled to SLR
(Tiwari et al. 2024) MODFLOW-SEAWAT	Mediterranean coastal plain (Metaponto Plain, Italy)	✓	✓	Transient SLR (until 2100) + salinity rise	×	EURO-CORDEX (non-CMIP) 6 RCMs*	6	CMIP-5 RCP4.5/8.5	Decadal	Decadal recharge & SLR	Decadal socio-economic abstraction scenarios	No land-surface hydrology model; CMIP-5
(Reinecke et al. 2021)(stand-alone recharge)	Global scale GHMs*	×	×	—	—	8 GHMs* × 4 CMIP-5 GCMs	4	CMIP-5 RCPs 2.6–8.5	Monthly	Monthly	Global multi-model recharge ensemble	No site detail, no SLR, no density
(Barnard et al. 2025–MODFLOW-NWT	Regional coastline, Southeast US	×	✓	Intermediate scenario from the IPCC	✓ (beach loss, subsidence)	CMIP-6	3	SSP1-2.6 to 8.5	—	N/A	Multi-hazard layering incl. shallow GW rise	Steady-state simulations; broad scale
(Ashofteh et al. 2025) MODFLOW + Bayesian GCM blend	Inland basin, aquifer in Iran	×	×	—	—	5 CMIP-3 GCMs + hybrid	5	SRES A2/B2	Monthly	Discrete SLR increments (0.25–3 m); no transient recharge coupling	Bayesian weighting of GCMs for GW forecasting	Inland; no SLR, no density
(Sathish et al. 2022)FEFLOW 3-D	Narrow dune-barrier aquifer ($35\ km^2$, SE India)	✓	✓	GHB + constant sea nodes raised linearly at 1, 2, 5 $mm\ yr^{-1}$	No	PRECIS RCM * (HadCM3Q0)	1	CMIP-3 (A1B emissions)	Monthly	Recharge: monthly SLR: annual linear head rise	Combines rainfall ↓, SLR ↑, pumping ± 10% on an island lens	Single RCM; No land-surface hydrology model; old CMIP-3
Our study – ESVA SWAT + SEAWAT(3D MODFLOW-MT3DMS)	Low-lying coastal peninsula, USA	✓	✓	Yearly GHB sea stage Increments (GHB), applied at the beginning of every decade	Partially (through land-fraction mask)	4 CMIP-6 GCMs (BCC-CSM2-MR, CanESM5, MIROC6, MRI-ESM2-0)	4	CMIP-6, SSP2-4.5 & 5–8.5	Annual stress periods from 2023 to 2080; each year subdivided into 4-time steps	Decadal recharge & SLR	• Multi-model recharge • couple CMIP6-driven SWAT hydrology with 3-D variable-density flow and explicit SLR-impacted GHB • land-surface fraction mask usage • Evaluates two SSPs (8 models + 2 ensemble means)• Freshwater volume variations	

[*] Asterisks denote abbreviations defined in the Abbreviations section.
[†] Such as marsh flooding, land loss, subsidence, etc.

2. Methodology

2.1. Study area

The ESVA study area lies within the Coastal Plain physiographic province and encompasses two counties, i.e., Accomack and Northampton (Fig. 1). This peninsula spans approximately 113 km in length and 16–32 km in width, covering about 1800 square kilometers of land. It is bounded by the Atlantic Ocean to the east, Chesapeake Bay to the west, and the state of Maryland to the north. ESVA is a low-lying peninsula (rarely exceeding 15 m (~50 feet) elevation), underlain by a surficial unconfined aquifer and three confined aquifers (see Fig. SF1; Supplementary Materials Fig.). The region experiences a humid subtropical climate, characterized by warm, humid summers and relatively mild winters. Rainfall is fairly consistent year-round, totaling approximately 1143 mm annually (Sanford and Pope 2007; Sanford and Pope 2010). Agriculture, including poultry production and processing, fishing, and tourism serve as the primary pillars of the local economy. Farmers in the region commonly grow crops such as corn, soybeans, and several types of small grains, which are essential to the area's agricultural output (Smith, 2015).

The hydrogeologic setting of ESVA is characterized using lithologic and geophysical data analyses, as well as water-quality assessments (Fig. SF1 (Supplementary Materials Fig.); Sanford et al. 2009). The conceptual framework, originally established by Richardson (1994), delineates a surficial (unconfined) aquifer, three confined aquifers (the Upper, Middle, and Lower Yorktown-Eastover aquifers), each separated by confining units, and a basal confining unit known as the St. Mary's confining unit. For this study, we focus on the surficial aquifer for head variability, as it is a source of freshwater and is most sensitive to climate-driven recharge and sea-level rise. Variations in surficial groundwater levels also provide a key indicator of vulnerability for near-surface infrastructure, including onsite wastewater treatment systems, which represent the dominant form of wastewater management in the region. The unconfined surficial aquifer extends across the entire study area, with its base ranging from 0 to 30 m below sea level and a thickness varying between 0.3 and 24 m. It is primarily composed of yellow sand, sandy clay, and minor gravel deposits. Historically, this aquifer has provided adequate water for domestic and agricultural use; however, it is vulnerable to nitrate contamination from agricultural runoff in upland regions. Hydraulic conductivity is estimated to range from 10 to 30 m per day based on findings from Sanford et al. (2009). The base of the surficial aquifer remains fresh because it is underlain by the low-permeability Upper Yorktown–Eastover Confining Unit, which limits vertical flow and prevents seawater intrusion from the deeper saline units. This aquifer is replenished by rainfall recharge, especially over the central upland ridge of the peninsula. Fresh groundwater flows laterally from this recharge-rich upland toward discharge zones along coastal bays and tidal creeks. Because ESVA's terrain is almost flat, its fresh surficial groundwater thickness – and thus its salinity balance – is topography-limited. In other words, the water table is shallow, specifically near the coasts, so it cannot rise far above sea level without intersecting the land surface. When recharge exceeds the combined capacity of evapotranspiration and lateral groundwater drainage, the system responds through enhanced discharge to wetlands/tidal features, return flow, and localized surface saturation or ponding, rather than through unlimited increases in freshwater thickness. Beneath the surficial aquifer lies a sequence of confined aquifers and confining units. These aquifers are primarily freshwater, not naturally saline, and the confining units limit vertical flow, controlling both groundwater movement and solute transport (see Supplementary Table ST1). The upper Yorktown-Eastover confining unit, situated directly below the surficial aquifer, is relatively thick and exhibits low hydraulic conductivity, effectively restricting vertical water movement. Underlying this unit, the upper Yorktown-Eastover aquifer extends to depths of up to 91 m below sea level, with hydraulic conductivity values ranging from 0.03 to 23 m per day. Deeper in the stratigraphy, the middle and Lower Yorktown-Eastover aquifers, separated by additional confining layers, exhibit progressively lower hydraulic conductivity, attributable to increasing proportions of fine-grained sediments. The Lower Yorktown-Eastover aquifer reaches depths of approximately 150 m below sea level at its deepest point and has the lowest conductivity among the three, consistent with its finer sediment composition. The basal confining layer, the St. Marys confining unit, forms the lower boundary of the groundwater system and is characterized by extremely low hydraulic conductivity (~3.048×10^{-6} m per day), effectively limiting groundwater flow beyond this depth (Sanfordetal.,2009). In addition, subsurface paleochannels occur where erosional channels had incised the Yorktown Formation and been infilled with Pleistocene-aged marginal-marine deposits. The Exmore and Eastville paleochannels are prominent features within the study area, with depths exceeding 49 m and 37 m, respectively, and estimated sediment fill thicknesses of approximately 30 m and 18 m (Sanfordetal.,2009).

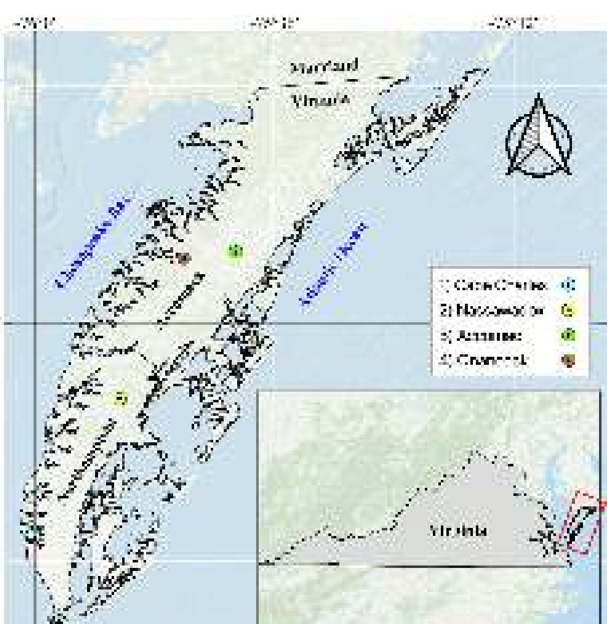

Fig. 1. Location and geographic extent of the Eastern Shore of Virginia (ESVA), showing Accomack and Northampton counties.

The groundwater-flow system on the Eastern Shore of Virginia (ESVA) is primarily driven by freshwater recharge occurring in the central upland areas, where water infiltrates and moves laterally through the surficial aquifer system. The estimated natural recharge is approximately 0.95 million cubic meters per day (0.83 mm/day) (Richardson, 1994). Sanfordetal.(2009) water-budget analysis further suggests that roughly 0.12 mm/day of this infiltration leaks downward through confining beds to replenish the deeper confined Yorktown–Eastover aquifers—a flux equivalent to ~15% of surficial recharge. Most groundwater flows toward the coastal bays, eventually discharging into the Chesapeake Bay or the Atlantic Ocean (Speiran, 1996). The water table (groundwater table[2]) exhibits spatial variability, with higher elevations in the central upland and lower levels near the coast. Groundwater extraction from pumping wells induces cones of depression, reducing hydraulic pressure, and increasing the risk of saltwater intrusion. However, water levels can recover if pumping is

[2] We use the term water table—the more common hydrogeologic term—to refer specifically to the groundwater table (the upper surface of the saturated groundwater zone), which is different from surface-water levels as used in wetland hydrology.

reduced or ceased (Sanfordetal.,2009).

2.2. Modeling framework

Fig. 2 shows the modeling framework developed in this study to evaluate the impacts of changes in recharge and SLR on groundwater dynamics. The modeling approach integrates key inputs, including hydrogeological data, climate projections, and spatial datasets such as Digital Elevation Model (DEM), land cover, soil types, and aquifer properties.

After running 58-year simulation periods (2023–2080), we assessed the combined effects of varying recharge rates and one scenario of sea-level rise on surficial groundwater storage, water-table elevations, and SWI in a confined layer. The analysis explored both spatial and temporal trends in groundwater availability, offering a comprehensive view of how these climate-driven factors could influence the ESVA's aquifer system in the long term. Groundwater withdrawals were held constant at 2023 rates in all simulations to isolate the impacts of climate variability and sea-level rise; climate-driven changes in demand were therefore not modeled. By examining model outputs across multiple future scenarios, we were able to identify key patterns and potential risks, highlighting the variability in spatial and temporal groundwater responses.

2.3. SEAWAT-based groundwater flow and transport model: configuration and updates

The ESVA groundwater model was originally developed by Sanfordetal. (2009) using SEAWAT2000 (Guo & Langevin, 2002; Langevinetal.,2003) to evaluate the effects of future water withdrawals on groundwater levels and salinity in the aquifer system. As we modified the VADEQ (2024) updated version of Sanford et al. (2009) model for our study, this section provides a summary of the original model, its framework, and previous updates (Poeter and Hill, 1999). The SEAWAT model grid extends beyond the Virginia border into Maryland and includes offshore zones within both the Chesapeake Bay and Atlantic Ocean to capture interactions between freshwater and saline groundwater systems (Sanfordetal.,2009). The model grid consists of 370 rows, 102 columns, and 46 vertical layers, with a horizontal cell size of 305 × 305 m (1,000 ft), following the calibrated regional SEAWAT model of Sanford et al. (2009) and the VADEQ (2024) approved calibrated model. This regional discretization is intended to resolve peninsula-scale hydraulic gradients, coastal discharge, and the density-driven freshwater–saltwater transition while maintaining computational feasibility. Recharge and evapotranspiration are applied at the land surface, coastal interactions are represented with general-head boundaries (with conductance scaled by fractional water coverage), and withdrawals are implemented as spatially distributed, temporally varying pumping stresses in the confined system. Additional details on discretization, land-surface assignment, boundary/initial conditions, and pumping representation are provided in the Supplementary Materials (2.3. SEAWAT-Based Groundwater Flow and Transport Model: Configuration and Updates; Fig. 3; Tables ST2 and ST3).

Fig. 3 shows the conceptual representation of hydrogeologic units and groundwater-flow processes in Virginia's Eastern Shore region.

The model showed good agreement ($R^2 = 0.93$) to aquifer water-tables, supporting its reliability for long-term simulations (Sanford et al., 2009). While the model provides reliable long-term water-level

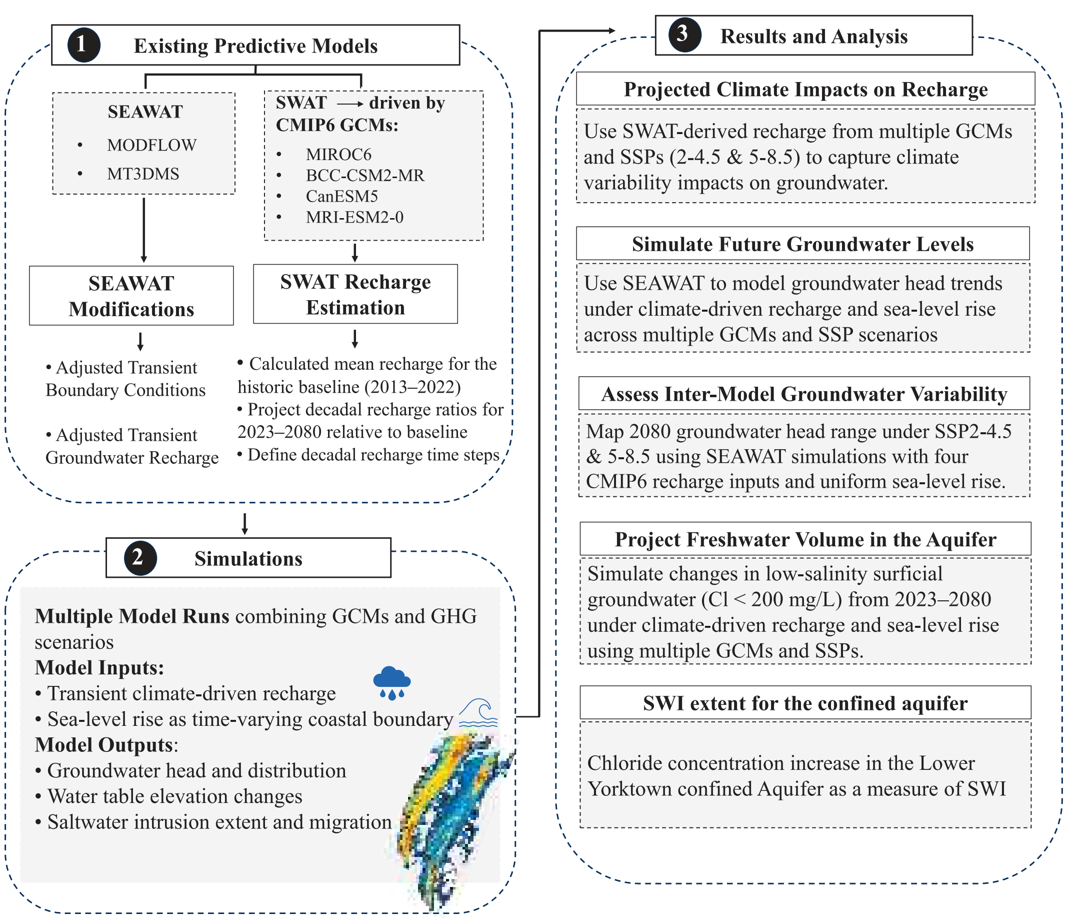

Fig. 2. Framework integrating climate projections, hydrogeological data, and spatio-temporal datasets to simulate groundwater responses to recharge variations and SLR over 2023–2080.

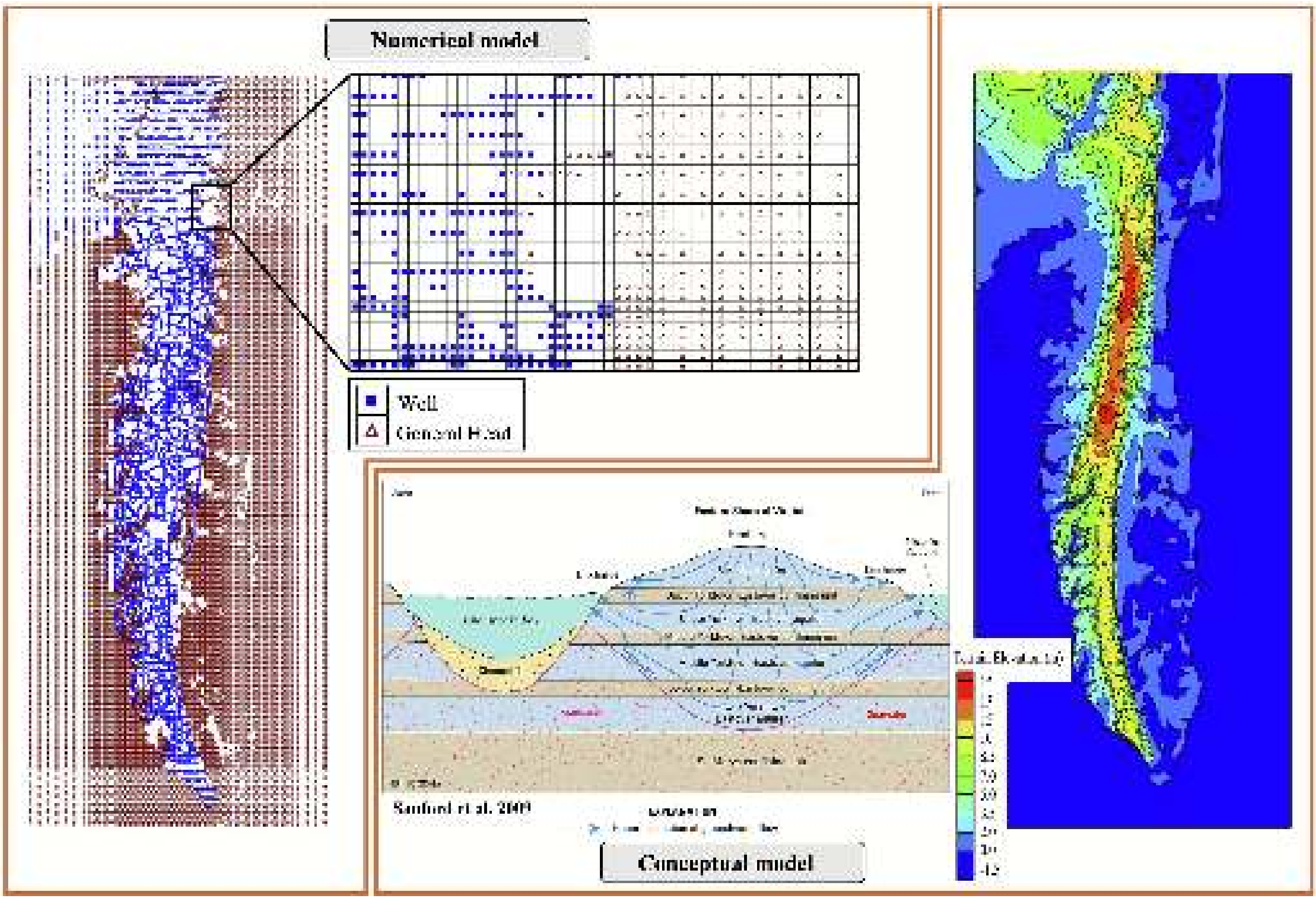

Fig. 3. Conceptual representation of hydrogeologic units and groundwater-flow (adapted from Sanford et al., 2009) along with graphical representation of the SEAWAT groundwater model.

predictions, salinity forecasts have been interpreted with caution due to greater uncertainty in transport simulations (Sanford et al., 2009). Table ST2 summarizes the model configuration, boundary conditions, calibration approach, and key performance metrics. Further details are available in Sanford et al. (2009).

In 2010, the Sanford et al. (2009) model was selected by VADEQ as the regulatory model for groundwater permitting on the ESVA (VADEQ, 2024). Additional water withdrawal data and water-table observations were added from 2004 to 2015 to facilitate the first major recalibration to update the model (VADEQ, 2024). Since that time, annual updates have been performed based on incorporating recent observations and withdrawals to recalibrate the model, before performing 50-year future regulatory simulations. Our analysis uses the VADEQ 2024 updated model (VADEQ, 2024), with no additional calibration, to ensure consistency with the officially approved groundwater model.

2.4. Formulation of SWAT hydrological model for recharge changes

The Soil and Water Assessment Tool (SWAT) is a process-based, semi-distributed hydrologic model developed by the USDA Agricultural Research Service (USDA-ARS) (Arnold et al., 2012). Watersheds are partitioned into subbasins and then into Hydrologic Response Units (HRUs) defined by unique combinations of topography components, including DEM, land use/land cover (LULC), soil, and slope. SWAT has been widely applied, with example applications including quantification of land-use impacts (Saber & Sumi, 2023), assessment of climate-change effects (Marshall et al., 2025), and evaluation/validation of remotely sensed products (Nguyen et al., 2023; Le et al., 2023; Aryal et al., 2023).

In this study, SWAT is used to project future changes in groundwater recharge for 2023–2080 under multiple GCMs and SSP scenarios (Section 2.2; Fig. 2). The SWAT model was adopted from Tran and Lakshmi (2024), in which QGIS v3.16.9 was used to perform the model setup (Dile et al., 2016), with watershed delineation using TauDEM v5.0 (Tarboton, 2011). However, we found that automatic watershed delineation has uncertainties due to the area's low relief and small size; many small, disconnected streams in ESVA are difficult to delineate (see Supplementary Fig. SF2). Therefore, the traditional workflow was modified to improve stream extraction across ESVA by testing seven DEM products. We found that the 90-m MERIT DEM (Yamazaki et al., 2019) provided the best stream-network delineation and was adopted in this study. We also validated the stream network against HydroRIVERS (Lehner & Grill, 2013) and Google Earth imagery to ensure our model's accuracy.

For precipitation, precipitation dataset (i.e., from the National Oceanic and Atmospheric Administration (NOAA); https://www.ncei.noaa.gov/maps/daily/) was collected; however, we anticipate that this might introduce noise and gaps in rainfall data due to tidal influences, which frequently occur in coastal regions. Indeed, these stations (i) are located next to the shore, which might be strongly affected by coastal influences, and (ii) have a limited number of available gauges with significant gaps, making them potentially unsuitable for representing precipitation patterns over the entire watershed. Specifically, only 3 rainfall stations out of the total 14 (see Table ST6) have sufficient data for quantifying uncertainties in GCMs' historical precipitation, but not for the SWAT simulation period (2001–2020). We then decided to use the remotely sensed product – NASA GPM IMERG Final Run V6 –

which has been bias-corrected for U.S. conditions (Hou et al., 2014).

For model calibration and validation, USGS gauges (2003–2020) data were used at the Pocomoke and Nassawango stations (Fig. 4c). A key limitation was the lack of streamflow observations over ESVA. Specifically, there is currently no long-term, high-quality streamflow data observed for the ESVA (see Fig. SF3). In the USGS database, the three current stations located in the ESVA region measure ocean water surface elevation, wind speed, and direction, but not streamflow. Thus, we decided to extend the SWAT model setup to include the state of Maryland to obtain streamflow observation data (2001–2020) from the Pocomoke station (USGS-01485000) and the Nassawango station (USGS-01485500). We selected the first two years (2001–2002) as the warm-up period, followed by a calibration period (2003–2013) and a validation period (2014–2020). We conducted 1000 calibration iterations with 23 parameters (Supplementary Table ST4) on a daily scale using the interactive R-SWAT web application (Nguyen et al., 2022) and the Sequential Uncertainty Fitting (SUFI-2) algorithm (Khalid et al., 2016). The SWAT model performance was evaluated using the Kling–Gupta efficiency (KGE; (Guptaetal.,2009), Nash–Sutcliffe efficiency (NSE; Nash & Sutcliffe, 1970), and the coefficient of determination (R^2; Moriasi et al., 2015). The equations and acceptable ranges for these metrics are provided in Supplementary Table ST5.

2.5. Integration of climate-driven recharge projections using bias-corrected GCM outputs

The recharge rates are extracted under two greenhouse gas (GHG) emission pathways from four GCMs. Specifically, our work continues the

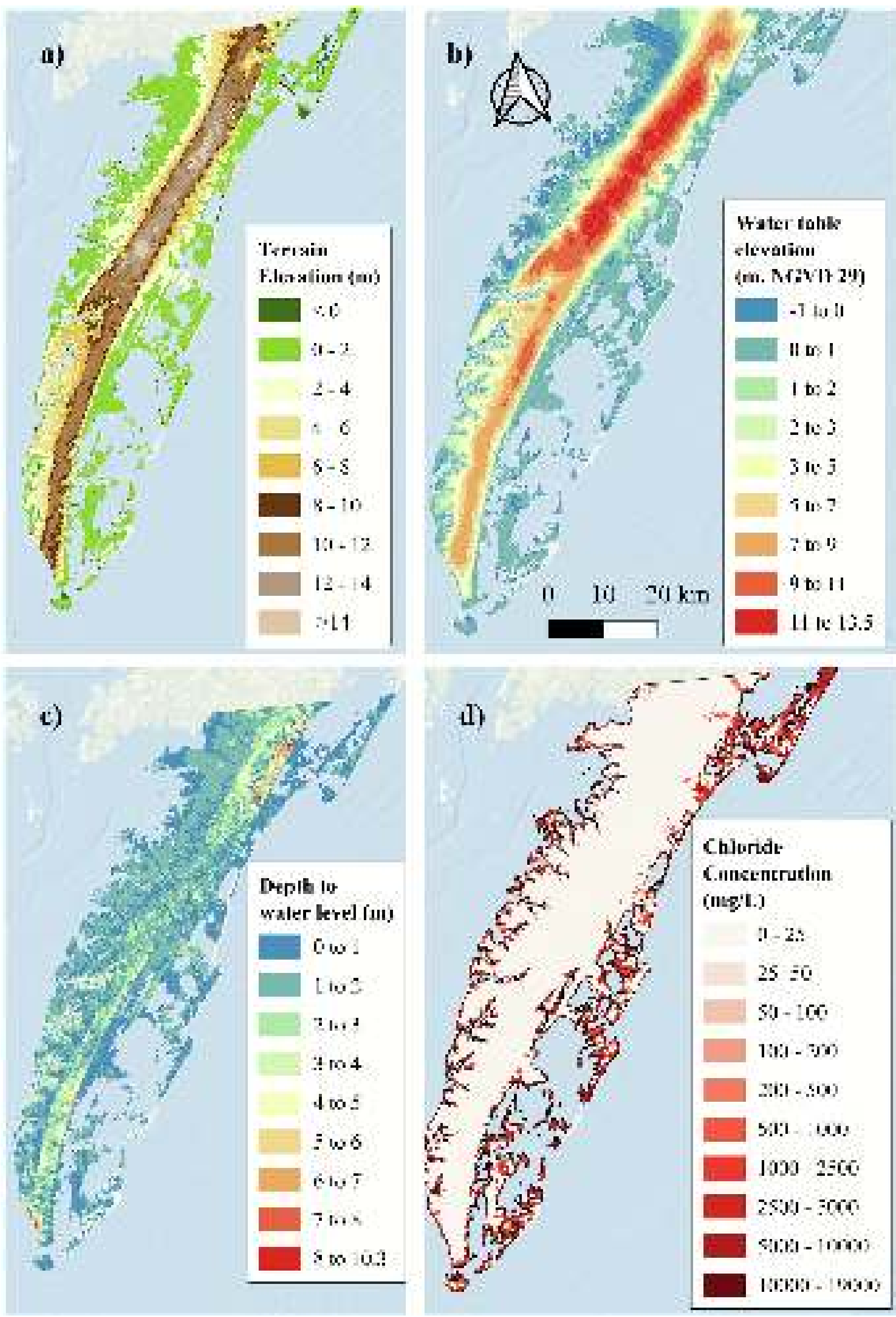

Fig. 4. (a) shows terrain elevation (m, NGVD 29), (b) simulated water-table elevation (water level) in the surficial aquifer (m, NGVD 29), (c) illustrates the depth to groundwater (m), (d) initial chloride concentration (mg/L).

work by Tran and Lakshmi (2024) in which they investigated the impacts of hydrological extremes over the entire ESVA using the SWAT model (Arnold et al., 2012) and GCMs. The projected inputs for SWAT (i.e., precipitation and temperature) were derived from GCMs, which were employed from the BCSD (Bias Correction and Spatial Disaggregation) method, a trend-preserving statistical downscaling algorithm (Maurer & Hidalgo, 2008) and downscaled to 0.25 degrees (~25 km) before use.

The four GCMs used are MIROC6 (Model for Interdisciplinary Research on Climate) by JAMSTEC (Japan Agency for Marine-Earth Science and Technology), BCC-CSM2-MR (Beijing Climate Center Climate System Model V2) by Beijing Climate Center (BCC), China Meteorological Administration, CanESM5 (Canadian Earth System Model V5) by Canadian Centre for Climate Modelling and Analysis, and MRI-ESM2–0 (Meteorological Research Institute Earth System Model V2) by Meteorological Research Institute (MRI) of Japan Meteorological Agency. These models are selected due to their effectiveness in capturing high variability in meteorological conditions, the importance of which was also highlighted in previous works, e.g., Parketal.(2023), Nguyenetal. (2024), Thrasheretal.(2022), and Tran etal. (2024b), with more details found in Tran & Lakshmi (2024). Specifically, these four models exhibit particular strength in simulating streamflow variations, as documented across several validation studies (Chen et al., 2022; Peng et al., 2023; Xu et al., 2023). Wang et al. (2021) demonstrated that both CanESM5 and BCC-CSM2-MR yield reliable outputs for key hydrological variables including precipitation patterns, evapotranspiration rates, and soil moisture content. Additionally, Peng et al. (2023) identified MIROC6 and MRI-ESM2–0 as exhibiting superior performance in modeling temperature and precipitation dynamics compared to alternative GCM options.

Following the framework established by Thrasher et al. (2022), for scenario analysis, this research employs two GHG emissions pathways: an intermediate emission pathway (SSP2–4.5) and a high emission trajectory (SSP5–8.5).

Given the four previously described GCMs and two GHG scenarios, the SWAT watershed model was used to determine 8 sets of groundwater recharge rates. In total, we analyze 11 recharge forcings: the eight individual GCM members (4 under SSP2-4.5 +4 under SSP5-8.5), plus three composites: (i) the ensemble average recharge for SSP2-4.5, (ii) the ensemble average recharge for SSP5-8.5, and (iii) a current baseline recharge scenario. For each set, relative changes in groundwater recharge rates were estimated by calculating the ratio of future predicted recharge rates relative to the average recharge during a 10-year baseline period (2013–2022) (Fig. SF4). These recharge ratios (future recharge relative to 2013–2022 recharge) were calculated for the initial seven-year period (2023–2030) and at each subsequent 10-year interval (2031–2040, 2041–2050, etc.) through 2080. This method aligns with the predictive model's simulation horizon (2023–2080). To integrate these projections into the hydrological modeling framework, values in the recharge input file of the SEAWAT model were multiplied by the recharge ratios at each stress period to reflect anticipated climate-driven variability in recharge.

2.6. Revisions to groundwater model

This study began with the Sanford et al. (2009) model updated for the VADEQ to 2022 without repeating the long history of model calibration. This section describes the changes made to incorporate climate forcing. The predictive version of the groundwater model was used to simulate future conditions over a 58-year period (2023–2080). We modified the model to account for projected changes in precipitation and temperature by transitioning from a constant to a transient recharge framework. Transient recharge forcing was derived from SWAT daily simulations (2001–2080) by converting SWAT groundwater-recharge outputs into decadal recharge ratios (relative to 2013–2022) and applying these as multiplicative updates to the spatially distributed MODFLOW recharge field at the start of each decade. Climate projections are first translated into spatially distributed recharge changes based on soil permeability and land-surface slope, assigning higher recharge to well-drained uplands and lower recharge to poorly drained coastal or marsh zones. These are then applied as time-varying transient stresses in the MODFLOW recharge package by updating the recharge field. Spatially variable recharge rates were updated at the beginning of every decade to better capture the temporal variability driven by climate projections. To represent future SLR on the ESVA, we applied a time-varying General-Head Boundary (GHB) condition to incorporate projected sea-level changes and salinity. For the ESVA coastline, we updated recharge and coastal boundary heads at decadal intervals to match the stress-period structure and applied a linear increase rate of 4 mm/year, based on long-term observational data from NOAA Tides and Currents Station #8632200 at Kiptopeke, Virginia (NOAA, 2024). Historical records from 1951 to 2024 indicate a relative sea-level trend of 4.03 ± 0.29 mm/year, corresponding to an estimated rise of approximately 0.4 m (1.32 ft) over a 100-year period.

In the model, SLR was incorporated as a time-varying boundary condition applied to the coastal boundary cells. All cells with land-surface elevation ≤ 1 m (all barrier islands, marsh fringe and tidal creeks) from the vertical control datum are specified as General–Head Boundaries (GHB). Beginning with a baseline year of 2023, the sea-level datum assigned to the GHB is raised by 4 mm/yr and updated at the first stress-period of each decade (2031, 2041, …, and 2071). Conductance values are left unchanged, so the inland hydraulic gradient responds naturally. Then, these incremental rises were added to the general boundary heads (GHB) in the model, allowing the boundary conditions to reflect projected sea-level increases over the simulation period. This approach mirrors the transient boundary head condition adjustment method employed by Tiwari et al. (2024), who also used decadal sea-level increments in their aquifer model, and enables dynamics simulations migration of saltwater intrusion, shifts in hydraulic gradients, and adjustments in the freshwater-saltwater interface under anticipated sea-level conditions. See Appendix in Supplementary Materials for more info about the SEAWAT packages used. These enhancements provide a more comprehensive evaluation of the potential impacts of climate change on groundwater resources in ESVA.

3. Results

3.1. SWAT calibration and validation

After 1000 runs for SWAT model calibration and validation, the daily-scale model performance for 2003–2020 produced satisfactory streamflow skill scores (Supplementary Fig. SF5), evaluated using model performance metrics (see section 2.4, Supplementary Table ST5, and Tran and Lakshmi, 2024 for details). Specifically, for Pocomoke, the model achieved the overall NSE = 0.56, $R^2 = 0.56$, and KGE = 0.62 (Fig. SF5a); for Nassawango, NSE = 0.58, $R^2 = 0.61$, and KGE = 0.58 (Fig. SF5b). We then use this calibrated model to simulate future changes in streamflow under four different GCMs and two SSP scenarios (see section 2.5), which will then be extracted and used as projected recharges for the SEAWAT model.

3.2. Uncertainties of GCMs

While future projections for precipitation and temperature vary widely across GCMs, it is important to assess how well GCMs' historical data, particularly precipitation, align with actual observations (in this case, the gauge bias-corrected IMERG Final product; see section 2.4). However, we anticipate that the validation may not yield a strong correlation (e.g., $R2 > 0.5$) due to several reasons. The IMERG product is satellite-based and monthly gauge-corrected (Hou et al., 2014); however, the limited number of operational gauges in this region (see section 2.4), along with the unique geographical setting of ESVA (15 m above mean sea level), may introduce uncertainties—an issue commonly observed in coastal watersheds (Derin et al., 2022; Le et al., 2023; Tran et al., 2024b). For example, Derin et al. 2022, when validating IMERG over U.S. coastal regions, reported that the product tends to overestimate light rainfall (<1 mm/h) and underestimate heavy rainfall rates (>10 mm/h) across all coastal areas. Moreover, rainfall was substantially overestimated near shorelines, particularly in regions closer to the coast.

After performing the uncertainty testing between IMERG and historical data from four GCMs (2001–2014), with rainfall stations located near the ESVA's shore filtered out to maintain a fair comparison, we obtained a summary for each GCM, as well as the Ensemble average, as shown in Table ST7. As expected, we found that the performance of these CMIP6 GCMs over coastal regions shows difficulties in capturing rainfall intensity, resulting in overall R2 values ranging between 0.30 and 0.36 (see Table ST7), similar to other studies by Srivastava et al. (2020) and Almazroui et al. (2021). Specifically, they indicated that CMIP6 GCMs exhibit reduced simulation accuracy in coastal zones due to complex land–sea interactions and topographic influences, leading to greater uncertainty in precipitation and temperature projections relevant to coastal hydrology and climate impact studies.

On the other hand, in coastal regions such as the ESVA, where (i) rainfall gauge networks are sparse and (ii) satellite-based rainfall products (i.e., IMERG) exhibit retrieval errors near coastlines (Derin et al., 2022), applying an additional bias correction, i.e., using the current four stations, on top of the existing bias-corrected IMERG, might introduce further uncertainty. Importantly, this added uncertainty could affect future hydrologic projections driven by GCMs. Given these potential issues, we decided not to apply an additional bias correction to the GCM precipitation datasets to avoid compounding uncertainties.

3.3. Projected impacts of climate variability on groundwater recharge

Climate change significantly influences groundwater recharge patterns. This section presents the projected groundwater recharge variations under different climate scenarios as extracted from SWAT. Table 2 summarizes the ratio of changes in groundwater recharge projected for each decade under both intermediate (SSP2-4.5) and high (SSP5-8.5) GHG scenarios across different GCMs.

During the first three decades, recharge projections under the high-emissions scenario (SSP5-8.5) exhibit approximately twice the coefficient of variation compared to the intermediate scenario (SSP2-4.5), indicating greater uncertainty and planning risk associated with high-emissions scenarios. The projections indicate varying impacts on GW recharge depending on the GCM and emissions scenario:

- BCC-CSM2-MR demonstrates a decline in recharge, with a significant drop under Intermediate GHG scenarios to 0.70 in 2071–2080.
- CanESM5 consistently shows the highest recharge ratios, particularly under high GHG scenarios, peaking at 1.62 in 2051–2060.
- The average of the ensemble projections exhibits a more stable trend, with values ranging between 0.97 and 1.06, indicating moderate climate impacts on recharge.
- During the first three decades, recharge projections under the high-emissions scenario (SSP5-8.5) exhibit approximately twice the coefficient of variation compared to the intermediate scenario (SSP2-4.5), indicating greater uncertainty and planning risk associated with high-emissions scenarios.

Table 2
Projected groundwater recharge ratios (projected recharge/baseline recharge) under SSP2-4.5 (intermediate GHG) and SSP5-8.5 (high GHG) scenarios.

Decade	MIROC6 (Int/High)	BCC-CSM2-MR (Int/High)	CanESM5 (Int/High)	MRI-ESM2-0 (Int/High)	Ensemble Avg(Int/High)
2023–2030	0.98/0.97	0.92/0.73	1.31/1.43	0.98/0.76	1.05/0.97
2031–2040	0.99/0.95	0.88/0.79	1.35/1.51	0.89/0.80	1.03/1.01
2041–2050	0.88/0.91	0.85/0.81	1.42/1.56	0.81/0.81	0.99/1.02
2051–2060	0.87/0.94	0.86/0.80	1.54/1.62	0.79/0.87	1.02/1.06
2061–2070	0.95/0.89	0.87/0.90	1.48/1.44	0.82/0.93	1.03/1.04
2071–2080	0.96/0.88	0.70/0.93	1.49/1.29	0.87/0.85	1.00/0.99
Dominant Signal*	mildly drier	persistently drier	persistently wetter	drier	near-baseline

Note: Int refers to intermediate GHG emissions (SSP2-4.5), while High refers to (SSP5-8.5).

* Based on whether ≥4 of 6 decades are above or below 1.

Overall, inter-model differences among GCMs exceed the differences observed between high and intermediate greenhouse gas emission scenarios.

Model-to-model comparison of projected recharge ratios (pooled across all decades) reveals substantial differences in both magnitude and direction of change. The inter-model spread underscores an important insight: the current recharge values and ensemble average, while convenient, can obscure meaningful variations in recharge futures. CanESM5 and BCC-CSM2-MR are on the wet and dry ends, respectively, illustrating the importance of examining individual models when assessing adaptive strategies and groundwater vulnerability. The ensemble average hides this risk and therefore under-represents real uncertainty. Future projections should replace equal weighting of different GCMs for ensemble average with evidence-based weights (e.g., via cross-validation/Bayesian model averaging) once a more accurate climate product is identified for the site using future data. It should trigger a transition from equal weighting of climate models to weighting based on their predictive accuracy. These findings emphasize the importance of incorporating climate projections into groundwater resource management, particularly in regions dependent on GW for water supply. The varying recharge rates across models highlight uncertainties that need to be addressed through adaptive modeling and management strategies.

3.4. Projected water-table changes in the Eastern Shore surficial aquifer

Fig. 4b and 4c show the baseline (2023) water-table (NGVD 29, m) and the depth to water-table in the surficial aquifer, respectively. Since the surficial aquifer is unconfined, simulated groundwater head directly represents the water-table elevation (water level). In low-lying coastal areas where land-surface elevation relative to NGVD 29 is near or below 0 m, simulated water-table elevations may also plot near or slightly below 0 m, reflecting the vertical datum and regional topography. Depth to water-table averages around 1.5 m, while reaching 10 m in certain central, northern, and southern regions in the surficial aquifer.

The 2023 water-table serves as the baseline for comparison with different climate models. Groundwater extraction rates were held constant at 2023 levels across all future simulations to isolate the impacts of climate-driven recharge variability and SLR.

3.4.1. BCC-CSM2-MR scenario projections

Fig. 5 presents the projected groundwater level changes under the Intermediate GHG scenario using the BCC-CSM2-MR model, which represents the driest in the ensemble. The projections span five time slices—2030, 2040, 2050, 2060, and 2080. Positive values (blue) indicate a rise in groundwater levels, while negative values (red) indicate a decline. We applied a consistent color scale across all projections and time slices to enable direct comparison of Δh magnitudes; consequently, some drier scenarios do not populate the highest positive (wetting) classes, while wetter scenarios may not populate the most negative (drying) classes. From 2030 to 2080, the model projects a general

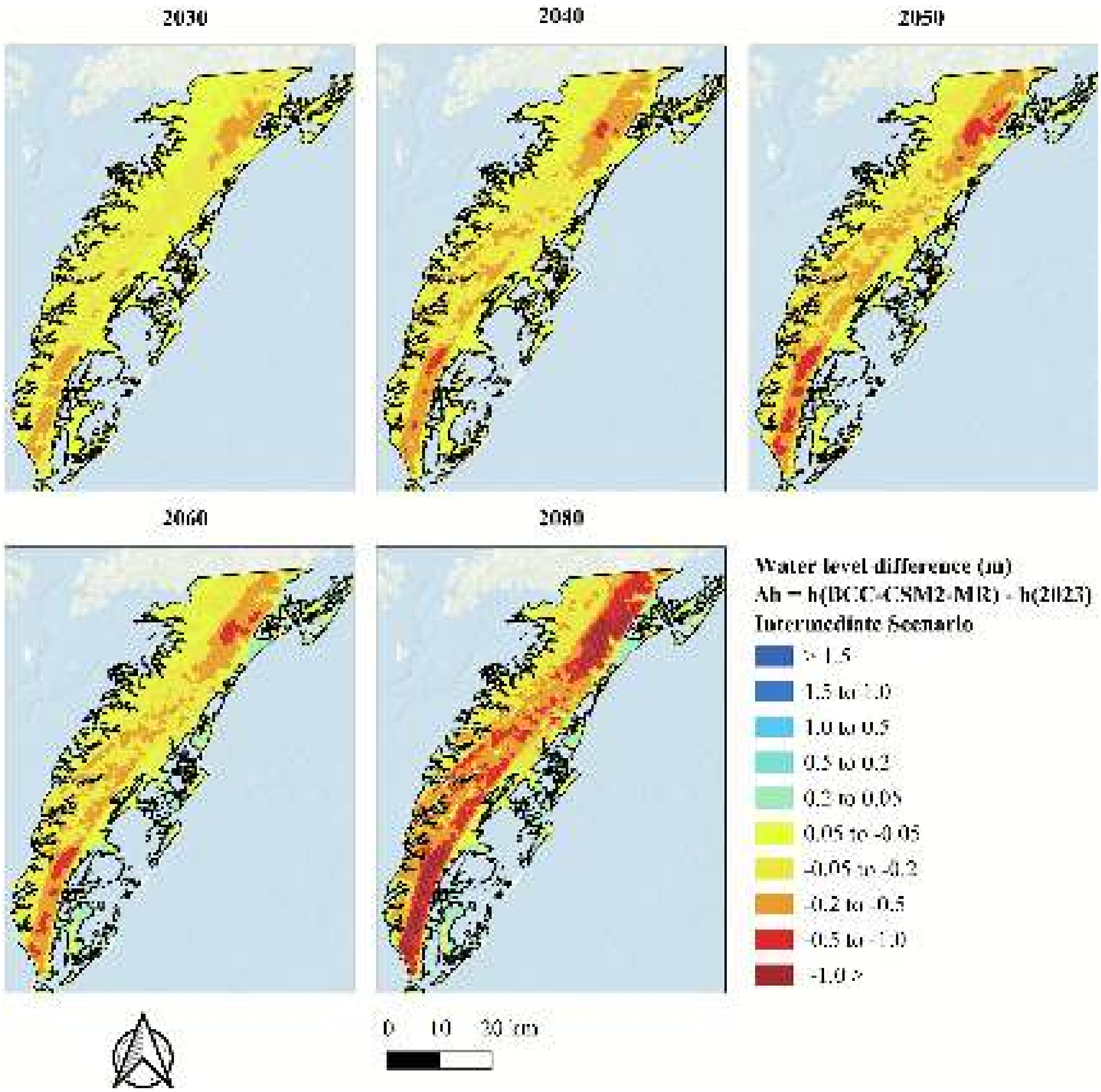

Fig. 5. Projected change in surficial-aquifer (Layer 1) head (Δh, m) relative to the 2023 baseline under the BCC-CSM2-MR Intermediate Scenario for 2030, 2040, 2050, 2060, and 2080.

decline in groundwater levels across the study area, with the most pronounced reductions occurring in 2080. By 2030, most inland cells already register declines of 0.05–0.20 m, while coastal fringe cells remain near steady state. Declines intensify through 2040 as simulated recharge decreases. By 2050, a continuous band of >0.5 m drawdown (purple red) forms along the peninsula's interior upland. Local interior areas exceed 1 m of head loss, indicating depletion of stored groundwater in the most recharge-dependent zones. The contraction of freshwater will continue by 2060. Much of the interior upland ridge records 0.5–1.0 m deficits, and by 2080 that band expands north–south, with several hotspots experiencing greater than 1 m drops. In contrast, barrier-island margins and the southern tip experience slight rising heads (yellow–light green) because the imposed sea-level-rise boundary partly offsets the recharge deficit there. Overall, the driest GCM in the ensemble transforms an early, modest decline across the peninsula into a late-century pattern characterized by significant interior drawdown alongside relatively buffered coastal zones. This highlights how reduced precipitation can surpass the effects of sea-level rise inland.

Groundwater declines are most pronounced in the peninsula's north-central and south-central zones. Between 2050 and 2060, the rate of drawdown slows slightly, but spatial differences grow considerably. By 2080, the interior upland ridge exhibits water-level declines exceeding 1 m, whereas isolated areas of head rise persist, indicating increasing spatial heterogeneity in hydraulic conditions.

Supplementary Fig. SF6 presents the projected groundwater level differences under the High GHG scenario using the BCC-CSM2-MR model. This scenario displays greater variability in both spatial and temporal groundwater responses compared to the Intermediate scenario. From 2030 to 2080, groundwater levels exhibit a wide range of changes. In the earlier decades (2030–2050), widespread areas—particularly in central and southern regions—show notable groundwater declines exceeding −1.0 m (indicated in red), with localized pockets of moderate rise in the north and coastal zones under the High GHG. The surficial aquifer first experiences interior drawdown where recharge lags behind pumping. By 2080, the extent of severe decline diminishes, and much of the region transitions to more moderate changes (yellow and light orange tones), suggesting potential groundwater stabilization or model-influenced recharge signals under this high-GHG trajectory.

These results underscore the heightened sensitivity of groundwater levels to both emissions intensity and model structure. The pronounced shifts in spatial patterns, particularly between 2040 and 2080, highlight the substantial role of high-emissions scenarios in shaping future water resource conditions and reinforce the importance of region-specific adaptation strategies that account for a wide range of climate futures.

3.4.2. CanESM5 scenario projections

Fig. 6 shows groundwater level projections under the Intermediate GHG scenario using CanESM5, which represents the wettest scenario in the ensemble. In contrast to BCC-CSM2-MR, CanESM5 simulates a general rise in groundwater levels throughout the region, primarily due to increased recharge. Localized increases reach up to 1.9 m, indicating increasing spatial heterogeneity.

The largest increases occur in low-lying inland areas, particularly in the central and southern portions of the domain, where recharge contributions dominate and groundwater mounding becomes more evident. Coastal areas, particularly near the shoreline, exhibit mixed responses. In the 2030s and 2040s, recharge surpluses increase water-table by 0.2–0.5 m (light blue cyan) across most uplands, while the axial interior corridor from Cape Charles to Onancock reaches 0.5–1.0 m (darker blue) by 2040. Only a few pumped centers remain within the near-zero yellow band. By 2050 (mid-century), head gains expand laterally. The interior upland ridge north of Exmore and sections of the southern neck exceed 1 m, and shallow coastal margins on both bay- and ocean-sides move decisively into positive territory, signaling that the recharge pulse is now overtaking the imposed SLR boundary. In 2060–2080 (late century), head increases intensify and spatial contrasts sharpen. By 2060, the central–northern interior shows contiguous 1–1.5 m increases, and isolated hotspots >1.5 m emerge near historic recharge maxima. By 2080, those gains extend right up to the barrier-island flanks, leaving only a few yellow slivers (<±0.05 m) where SLR still balances the wetter climate signal. Net coastal rise relative to sea level (blue fringe) implies a weakening of hydraulic gradients that normally drive saltwater inland.

The High GHG scenario (Supplementary Fig. SF7) intensifies these trends, with maximum increases exceeding 2 m and similarly wide variability. Compared to the Intermediate Scenario, the High scenario

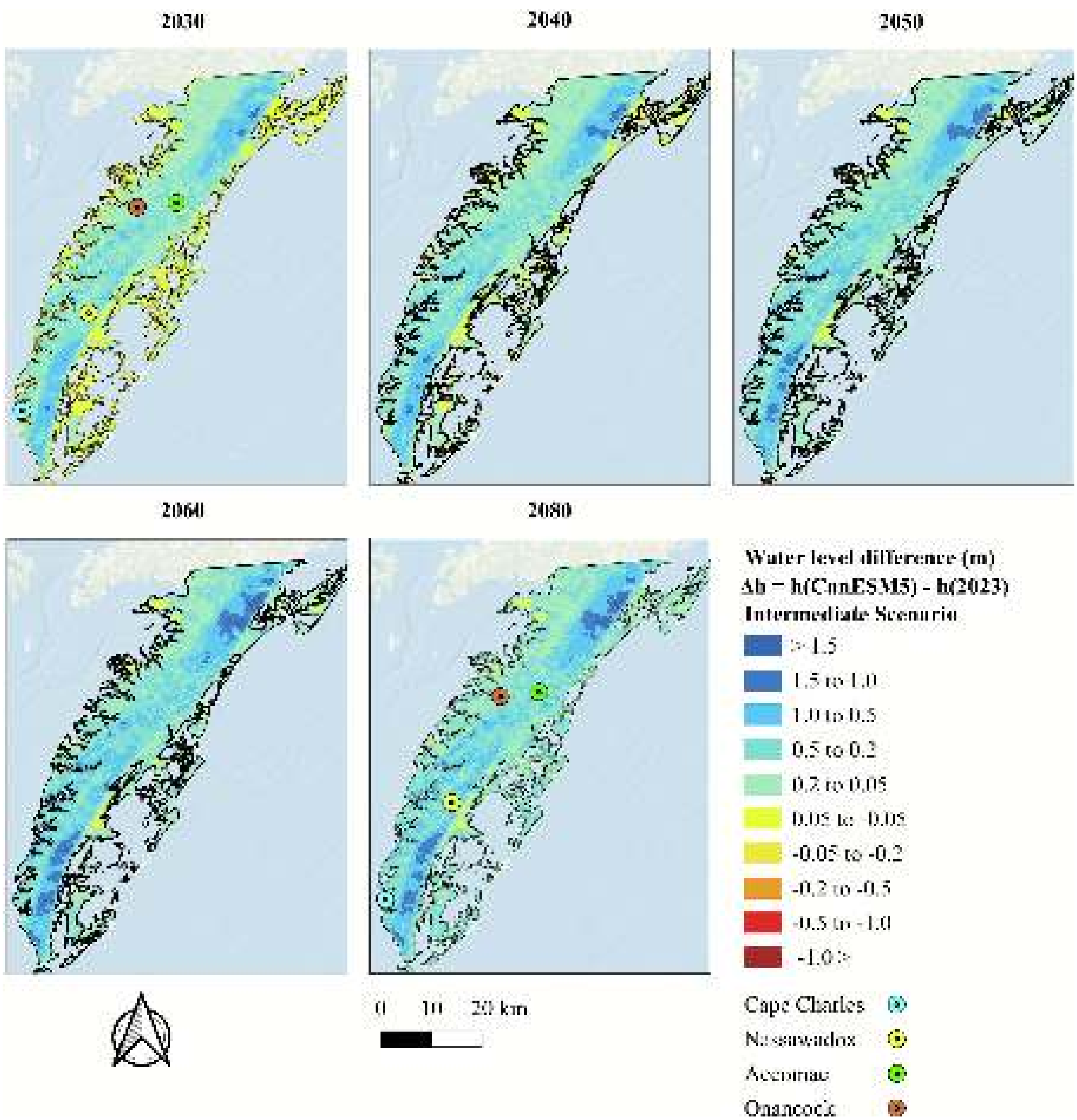

Fig. 6. Projected change in surficial-aquifer (Layer 1) head (Δh, m) relative to the 2023 baseline under the CanESM5 Intermediate Scenario for 2030, 2040, 2050, 2060, and 2080.

shows more extensive and pronounced increases in groundwater levels, particularly in southern and central regions, and until the mid-century, with even fewer zones of fixed heads along the coast. While this scenario suggests reduced groundwater depletion risk, it also raises concerns about waterlogging and infrastructure vulnerability in low-elevation urban zones in the early future decades. The increasing spatial variation of increased head further underscores the growing spatial divergence in hydrologic responses, suggesting the need for highly localized water management strategies.

Overall, CanESM5′s wet bias adds up to >1 m of additional storage in large interior tracts and upward heads of 5–20 cm along much of the shoreline, potentially mitigating salt-intrusion risk but heightening concerns about saturated soils around septic systems, croplands, and urban infrastructure. These findings illustrate the critical influence of recharge assumptions and call for infrastructure planning that accounts for both flood and drought risks under a range of climate futures.

3.4.3. MIROC6 scenario projections

Fig. SF8 illustrates projected groundwater level differences relative to the 2023 baseline under the MIROC6 intermediate and high GHG scenarios for the selected years. Under the Intermediate scenario, groundwater levels in 2030 remain relatively stable, with only small, localized decreases of about 0.10 to 0.20 m. By 2040, slight increases in groundwater levels begin to appear, particularly in central and southern regions, suggesting early signs of influence from SLR. In 2050 and 2060, a continued and more widespread decline in groundwater levels is observed, with larger areas affected and maximum decreases reaching up to 0.66 m. This pattern reflects a clear trend of groundwater depletion over time, particularly in the north-central and south-central regions, likely driven by reduced recharge rates during the 2040 s. However, by 2080, partial recovery of the water-table is noted.

Under the high GHG scenario, Fig. SF9 for 2030 shows slight initial declines in some regions, though most areas remain relatively stable. By 2040, more noticeable decreases in groundwater levels appear, especially in the core regions, indicating early impacts of a decline in recharge. In 2050, significant declines become evident, with large portions of the study area experiencing substantial reductions. By 2060 and continuing into 2080, severe and widespread groundwater depletion

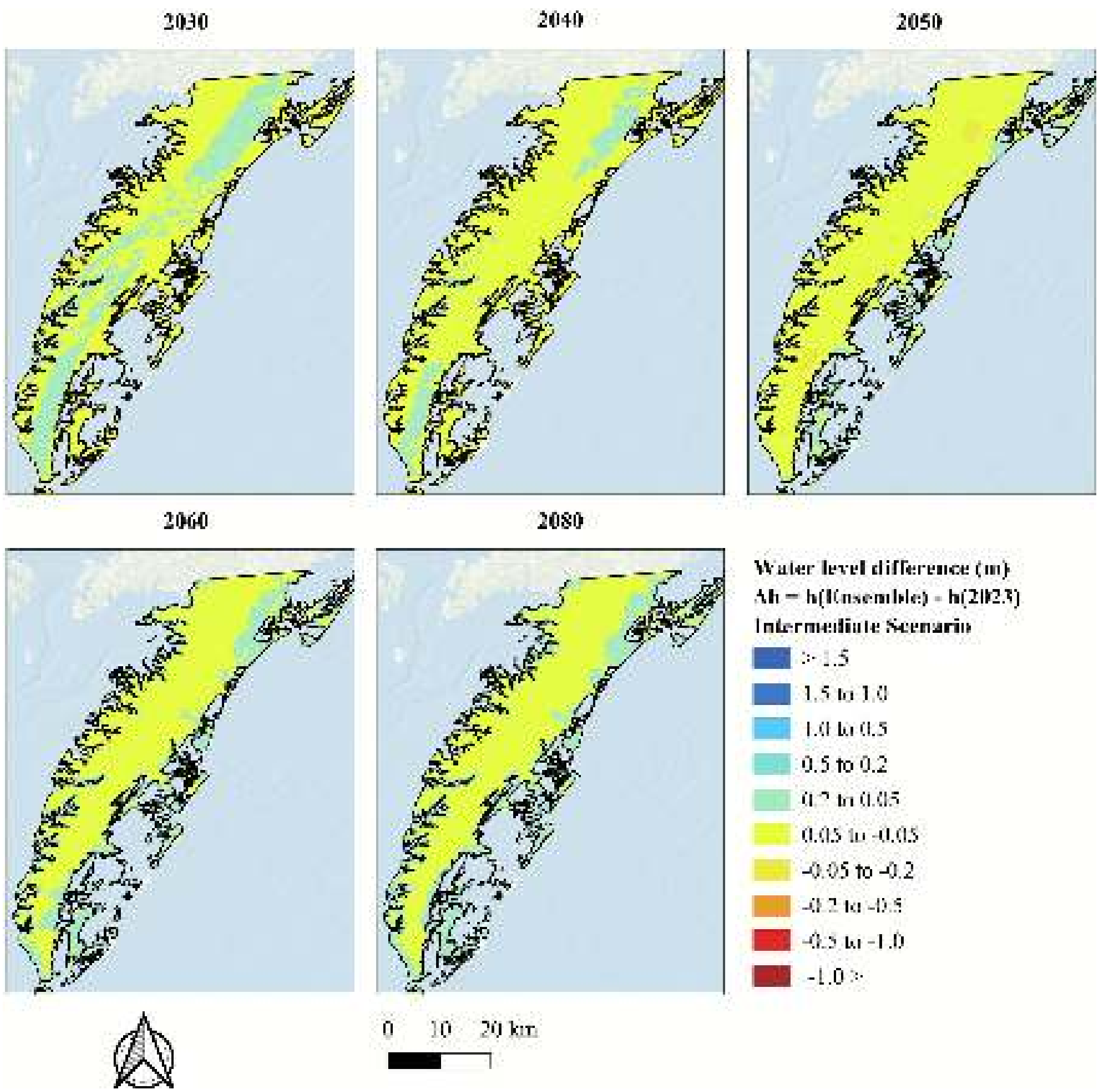

Fig. 7. Projected change in surficial-aquifer (Layer 1) head (Δh, m) relative to the 2023 baseline under the Ensemble Average Intermediate Scenario for 2030, 2040, 2050, 2060, and 2080.

occurs, with extensive areas showing substantial drops in groundwater levels, reflecting a serious reduction in groundwater resources under high-emission conditions. Additionally, the projections indicate an increase in the water-table at the shoreline location due to SLR.

3.4.4. MRI-ESM2-0 scenario projections

The groundwater level projections under MRI-ESM2-0 (Fig. SF10) exhibit trends similar to those observed under the MIROC6 scenarios, with progressive declines in groundwater levels through 2080. In 2030, almost the entire peninsula is in the neutral band. Only a few pumped centers in the south tip and one interior high point show modest declines. This is followed by a consistent increase in groundwater depletion, reaching depths of up to 1.1 m by 2060. A moderate recovery in groundwater levels is observed toward the end of the period, primarily concentrated along the coastline.

Under the high GHG scenario, Fig. SF11 displays a different trend. The spatial patterns show extensive areas marked in red, indicating regions at the highest risk of groundwater loss during the first three future decades (2030, 2040, and 2050), with maximum decline values reaching approximately 1.25 m. For 2060 and 2080, a slight increase in groundwater levels is projected, suggesting a potential stabilization or partial recovery in some areas.

3.4.5. Ensemble average scenario projections for two GHG emissions

Fig. 7 presents projected changes in groundwater levels in the surficial aquifer relative to the 2023 baseline, based on ensemble average recharge inputs for the intermediate GHG emissions scenarios and SLR. The ensemble average (i.e., giving each GCM equal weight) damps inter-model spread over ESVA, which is useful for context but may understate risk bounds. Under the ensemble average of the Intermediate GHG Scenarios, groundwater levels exhibit a modest increasing trend through mid-century, followed by spatial divergence. By 2030, widespread groundwater levels increases are projected across the coastal region, typically ranging from 6 to 12 cm, with localized gains exceeding 15 cm in the north and south-central zones—likely reflecting early responses to enhanced recharge. The upward trend persists in 2040 but weakens, particularly in central areas where projected changes approach zero, suggesting possible stabilization. By 2050, central and northern areas begin to show declines in groundwater levels, indicative of shifting recharge dynamics. The drying trend intensifies slightly by 2060, with declines up to 7 cm concentrated in central areas. Nevertheless, southern coastal zones maintain areas of groundwater rise, highlighting continued influence from SLR-driven boundary effects. By 2080, spatial variability becomes more pronounced. Southern portions of the region continue to experience increases exceeding 15 cm, while central and northern zones generally show mild declines, often remaining above baseline by approximately 3 cm. Overall, median head change remains within ± 0.05 m across the upland backbone for all decades.

In the High GHG scenario (Fig. SF12), 2030 projections show widespread declines in groundwater levels, particularly in the northern and southern regions, with reductions ranging from 14 to 18 cm. The remainder of the study area shows more moderate declines of up to 6 cm. By 2040, the pattern begins to shift, with slight increases (0–6 cm) across much of the region, potentially reflecting lagged SLR impacts and recharge variability. In 2050, coastal areas begin to exhibit notable increases in groundwater levels due to SLR, with projected gains ranging from 6 to 10 cm and localized peaks exceeding 20 cm. These increases become more widespread by 2060, particularly in low-lying coastal zones. Inland regions remain comparatively stable or continue to decline. By 2080, a reversal occurs in some inland areas, with renewed declines, while coastal zones sustain significant groundwater level rises (>20 cm). This spatial divergence underscores the contrasting hydrological responses between inland and coastal aquifers—driven by recharge limitations inland and SLR-induced pressures along the coast.

While the High Scenario projections show more pronounced regional changes than the Intermediate Scenario, ensemble-averaged results still indicate net changes of only a few centimeters (Fig. SF12). Large responses are attenuated by ensemble averaging, masking risks observed in high-variance projections from individual models. Nevertheless, even small changes in groundwater levels can have important implications for saltwater intrusion, ecological stability, and infrastructure resilience—particularly in low-lying, shallow aquifer systems.

4. Discussion

Distributional diagnostics of projected surficial-aquifer head changes (Δh) across CMIP6-driven recharge and emissions scenarios are provided in the Supplementary Materials (Section: Histogram-based interpretation of groundwater projections; Fig. SF16) to strengthen interpretation of the spatial patterns shown in Figs. 5–7.

4.1. Spatial distribution of model-to-model groundwater-level variation (2080, Intermediate GHG pathway)

Fig. 8 depicts the inter-model spread in simulated surficial-aquifer heads for 2080 under the intermediate (SSP2-4.5) GHG projection. The mapped statistic is the absolute range (max–min) of water-table elevation produced by the four CMIP6-driven recharge inputs (MIROC6, BCC-CSM2-MR, CanESM5, MRI-ESM2-0) after superimposing the common sea-level-rise boundary. Five classes (<0.25 m, 0.25–0.5 m, 0.5–1 m, 1–2 m, >2 m) illustrate how the magnitude of uncertainty differs across the peninsula. Fig. SF13 shows the same map for High GHG scenario in 2080 along with statistics.

The greatest variation in groundwater levels, exceeding 2 m in some areas, occurs along the peninsula's central spine (dark maroon). This

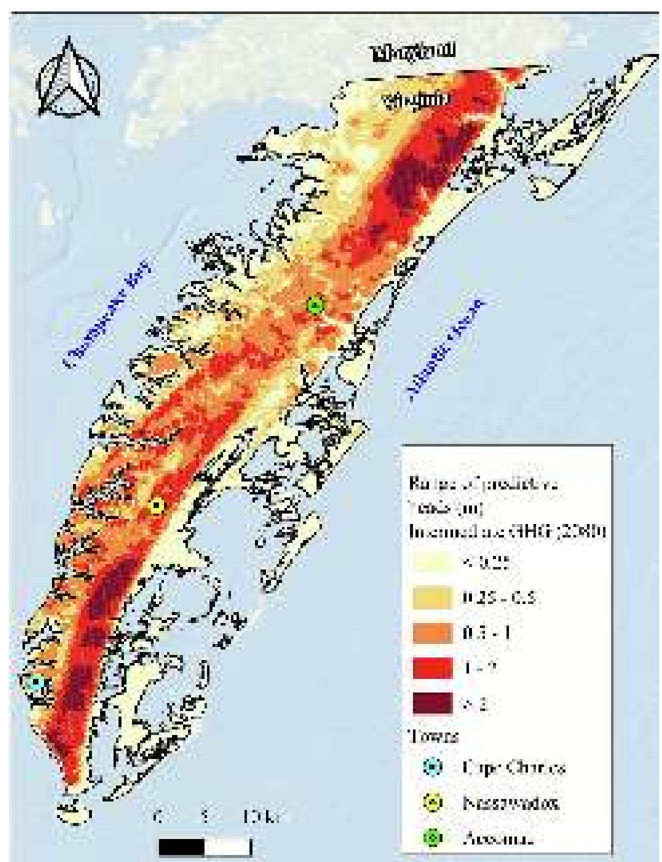

Fig. 8. Predicted groundwater head range (in meters) and statistics under the Intermediate GHG emission scenario for the year 2080. Areas in darker shades represent higher groundwater elevation ranges, while lighter shades indicate lower ranges.

zone coincides with the highest topographic elevations (Fig. 4) and the thickest vadose zone; model experiments show that recharge multipliers have a strong influence on changes in hydraulic head, particularly where the saturated thickness is greatest. Accordingly, the divergent precipitation signals of the wettest model (CanESM5) and the driest model (BCC-CSM2-MR) produce the widest bracket on interior heads. Placing monitoring wells along this sensitive ridge would provide an effective early warning system for future changes in aquifer recharge.

Moving away from the central ridge, orange-to-red bands (0.5–2 m range) appear along the Chesapeake Bay shore. Heads remain mildly sensitive to recharge, yet the aquifer thins toward the estuary, and a portion of the recharge signal is attenuated by the coastal general-head boundary representation. The result is a moderate yet still significant 0.5–1 m inter-model spread.

Barrier-island and back-bay cells are generally pale yellow (<0.25 m). In these low-lying areas, sea-level rise dominates hydraulic gradients, and all climate models impose the same time-varying sea-level boundary, effectively collapsing the spread. Recharge differences matter little because the saturated zone is thin and can equilibrate rapidly to boundary forcing.

Because inter-model head range exceeds 2 m along the interior upland ridge but is <0.25 m on barrier islands where SLR dominates, targeted monitoring should prioritize the high-variance ridge—installing nested piezometer clusters to track recharge trends and reduce projections uncertainty as new observations become available.

4.2. Water-table exceedance of land surface and associated land uses

Simulated heads in the surficial aquifer occasionally exceed land-surface elevation in low-relief portions of the ESVA, particularly under wetter recharge scenarios, reflecting topography-limited conditions where additional recharge is accommodated primarily through surface discharge rather than continued aquifer thickening. To evaluate whether these "super-elevated" cells occur in hydrologically plausible settings, we overlaid model cells with head > land surface against the Chesapeake Bay Program 2021 (1-m) LULC dataset (Claggett et al., 2025) and found strong spatial coincidence with wetlands, tidal marshes, ponds, and surface-water features (Fig. SF15). This agreement supports interpreting localized head exceedance as consistent with saturation/ponding and diffuse discharge in tidally influenced landscapes. A complementary sensitivity test implementing the MODFLOW DRN package in the surficial aquifer confirms that the study's main conclusions are robust to allowing explicit discharge where heads exceed land surface (full methods provided in the Supplementary Materials, 4.2. Water-table exceedance of land surface and associated land uses). SWI impacts and fresh groundwater volume analyses with drainage included are presented in the subsequent subsections.

4.3. Projected changes in fresh groundwater volume in the surficial aquifer

Freshwater storage was estimated by summing the volume of all model cells with chloride levels below 200 mg/L, the threshold for best quality potable water as suggested by Fidelibusetal.(2025). As salinity increases and cells exceed this threshold, they are excluded, tracking how saltwater intrusion reduces freshwater supply. A quick visual summary of the freshwater volumes is given in Fig. 9a. Lines show total fresh-groundwater volume (million m^3 (mcm)) produced by a common sea-level-rise boundary and 11 recharge forcings: four CMIP-6 GCMs (MIROC6, BCC-CSM2-MR, CanESM5, MRI-ESM2-0) run under Intermediate and High GHG scenarios, the ensemble averages, and a "Current Recharge" control with present-day recharge held constant. Divergence after 2030 is therefore attributable to climate-driven recharge change; upward trends denote expansion of the freshwater-saturated zone; downward trends denote thinning. As can be seen in Fig. 9a with unchanged recharge, the surficial aquifer saturated thickness decreases slightly, losing approximately 1 mcm per decade (−0.1% by 2080) with the imposed SLR. This trajectory is treated as the benchmark for assessing climate-driven changes in freshwater volume. Ensemble averages for intermediate and high GHG track the baseline case with small gains, suggesting moderate growth (slope: +1.1 mcm/decade and +0.4 mcm/decade, respectively). BCC-CSM2-MR with intermediate GHGs, which represents the driest scenario, experiences a sustained decline from 0.7% loss in 2030 to 2.5% by 2080 or −17.4 mcm volume/decade The wettest scenario, CanESM5 Intermediate, exhibits the most consistent and substantial increase in freshwater volume, reaching a +2.7% gain by 2080 and maintaining a growth rate of approximately +19.3 mcm per decade. Notably, the CanESM5 High scenario led all others in volume expansion up to 2060.

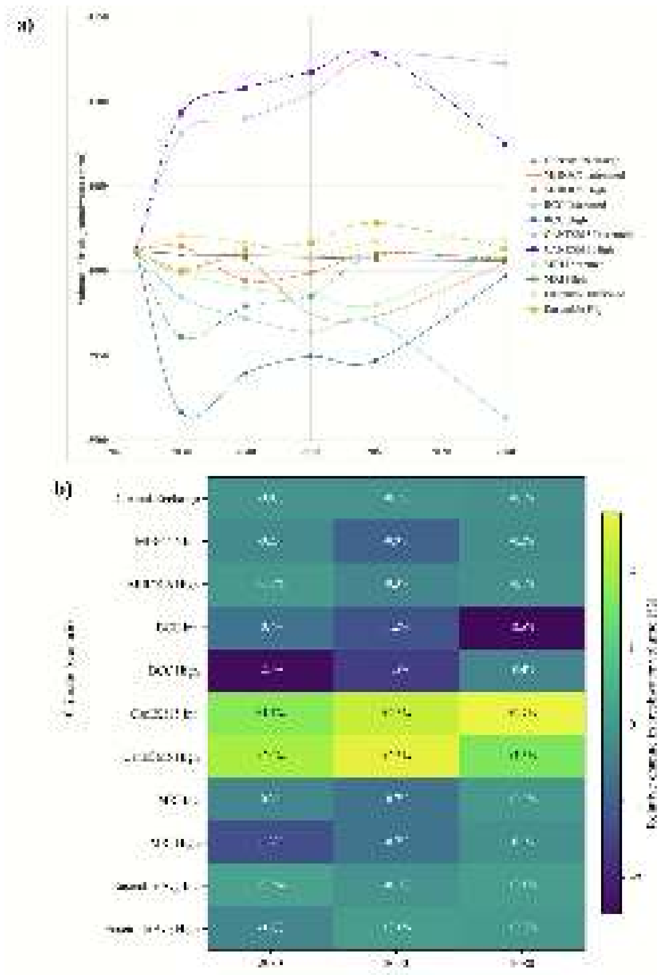

Fig. 9. (a) Time-evolution of the freshwater volume (Cl < 200 mg L^{-1}) in the surficial aquifer of Virginia's Eastern Shore, from 2023 to 2080. Dashed lines represent high GHG emission scenarios with square markers, while solid lines with lighter color represent intermediate scenarios with circular markers. (b) Relative change in freshwater volume (%) under various Climate Scenarios in surficial aquifer, sampled in 2030, 2050 and 2080. Warm colors (> 0%) indicate a larger fresh groundwater than in 2023; cool colors (< 0%) indicate contraction.

The heat map (Fig. 9b) shows the percentage change in low-salinity fresh groundwater volume (Cl < 200 mg/L) relative to the 2023 baseline volume of 4012 mcm. It highlights key trends across different climate models, with strong positive growth observed for the CanESM5 projections, represented by yellow-green colors. These indicate substantial increases in low-salinity surficial groundwater volume under this model because of higher recharge rates. In contrast, the BCC-CSM2-MR High (BCC High) and MRI-ESM2-0 High (MRI High) scenarios exhibit severe early losses, shown in dark blue, indicating significant declines in freshwater volumes, particularly in the initial decades. These variations reflect the differing impacts of recharge variation projections under each model scenario.

The direction and magnitude of simulated changes in surficial fresh groundwater storage and salinity are governed by shifts in the aquifer-system water balance and the hydraulic gradients that control coastal exchange. Storage changes reflect the balance between recharge inputs and head-dependent outputs (evapotranspiration, coastal discharge through general-head boundaries, and pumping). Under wetter climate projections (higher net recharge), water-table elevations rise, increasing saturated thickness in the unconfined surficial aquifer, and producing a net gain in freshwater storage. Conversely, under drier projections (reduced recharge), inland heads decline, discharge to coastal boundaries weakens, and freshwater storage decreases because less water is available to sustain the water-table and replenish the confined system through vertical leakage.

Projections based on individual climate models show notable variability. The CANESM5 scenarios predict relatively higher fresh groundwater volumes compared to other models, consistently maintaining levels above 4080 million cubic meters (mcm) after 2030. The MIROC6 model shows moderate stability under both Intermediate and High scenarios, with groundwater volumes fluctuating around 4000 MCM throughout the projection period. In contrast, the BCC Intermediate scenario projects a continual decline in groundwater volume, reaching the lowest value, approximately 3913 mcm, by 2080 among all cases studied. MRI-ESM2-0 projections under both Intermediate and High GHG emissions pathways exhibit an initial decrease by 2030, followed by a gradual recovery.

The ensemble projections, which average the outputs across models, reveal relatively stable trends. Both the Intermediate and High Ensemble Average scenarios indicate slight increases over time. Overall, while individual models display significant variation, the ensemble results suggest that future groundwater volumes will likely remain relatively stable. However, only the current recharge scenario and, to a lesser extent, the MIROC6 projections align with the ensemble averages, highlighting the importance of using multiple climate models in groundwater sustainability assessments.

Although a $\pm 2.5\%$ change in the freshwater volume appears small, the baseline aquifer contains $\sim 4 \times 10^9$ m^3 of freshwater. Supplementary Table ST1 summarizes water use and availability on Virginia's Eastern Shore. It compares the estimated freshwater volume with current residential and total water demand. The region uses about 20.7 million m^3 of groundwater annually, while residential use accounts for roughly 6.35 million m^3 (U.S. Census Bureau, 2021; USGS, 2021). A 2.5% loss ($\approx$100 million m^3, or 26.4 billion gallons) equals roughly five years of today's total groundwater withdrawals (public + agriculture + industry) on the Eastern Shore, or a full year's domestic supply for a population 15.7 times larger ($\approx$ 724,000 people). This puts the seemingly modest percentage change into a regionally significant context.

4.4. Inter-model spread and temporal evolution

Fig. SF14 shows the predicted freshwater volumes over time from the 11 models described in Section 4.3. Boxplots show median and spread of freshwater volume (mcm); overlaid points represent individual model outputs. While the ensemble average median shows a modest increase of just +0.1% from 2023 to 2080, the range of model outputs expands significantly over time. This muted trend conceals a two-fold growth in all 8 models inter–quartile range (IQR), from 25 MCM in 2030 to 46 MCM by 2060, indicating that uncertainty, not mean change, dominates the projection envelope. By 2080, the gap between the wettest (CANESM5-Intermediate: +110 MCM) and driest (BCC-Intermediate: –99 MCM) scenarios reaches 209 MCM. This variability reflects differences in model structures and hydrologic sensitivities.

Freshwater volume projections show evolving variability patterns across decades. In 2030 and 2040, scenarios under high GHG emissions (e.g., CanESM5 High, MRI High, and BCC High) exhibit notably greater spread than their intermediate counterparts, with outliers reaching both higher and lower extremes. This reflects a more uncertain and divergent response to climate forcing in the near term under high GHG scenarios. After 2060, however, the variability under high GHG scenarios begins to compress, especially in models like BCC High and MRI High, while the intermediate scenarios—particularly BCC and CANESM5 Intermediate GHG scenarios —maintain or widen their range. This pattern continues through 2080, where the ensemble average intermediate scenarios contribute to an increasing spread, suggesting persistent uncertainty in moderate pathways. In contrast, the High GHG scenarios become more clustered over time, indicating a convergence in projections despite more intense forcing. Overall, variability under high GHG pathways peaks around mid-century and narrows thereafter, whereas intermediate scenarios show a broader and more persistent range in projected freshwater volumes throughout the century.

4.5. Impacts of sea-level rise and recharge reduction on ESVA groundwater salinization

The surficial aquifer is the sole unconfined unit and provides baseflow to streams and wetlands, and recharges to lower layers. It contains fresh groundwater and is the uppermost layer of the model. In inland areas, head increases are primarily driven by changes in recharge, with minimal direct SLR influence. In coastal zones, however, SLR modifies the seaward general-head boundary, raising coastal water levels and initiating localized changes in hydraulic gradients near the shoreline. Once this boundary head increases, the compounding effects of reduced recharge and SLR propagate chloride concentration increase in the aquifer. However, chloride increases in the surficial and Upper Yorktown aquifers remain small, with most inland cells showing less than 1 mg/L of change and coastal fringe areas remaining below ~10 mg/L. These shallow aquifers experience substantially smaller salinity responses than deeper confined units because inland hydraulic gradients remain strong and the freshwater thickness is large relative to the magnitude of SLR imposed. In addition, hydraulic connectivity with surface features such as marshes and wetlands promotes drainage and limits sustained salt accumulation. In contrast, the Middle and Lower Yorktown-Eastover aquifers exhibit more pronounced chloride rises, particularly around Cape Charles, Willis Wharf (Southeast of Exmore), and Chincoteague. The confined Yorktown–Eastover aquifers on the Eastern Shore of Virginia are generally more vulnerable to seawater intrusion than the shallow surficial aquifer because they are hydraulically isolated from direct recharge and rely primarily on vertical leakage through overlying confining units. Recharge to these confined units is therefore lower than recharge to the surficial aquifer, making them more sensitive to long-term pumping stresses (Smith, 2015); Sanford et al. (2009)). Historical groundwater withdrawals from the Yorktown–Eastover aquifer system have exceeded natural recharge by approximately 1 million gallons per day, resulting in sustained declines in hydraulic head and increased susceptibility to saltwater intrusion (Smith, 2015). Among the confined units, the Lower Yorktown–Eastover aquifer is the most impacted because it is the deepest and thickest confined aquifer in the ESVA groundwater system, lies closest to regional saltwater sources, and experiences the greatest reduction in freshwater hydraulic gradients under pumping and sea-level rise (see Fig. SF1). Fig. SF17 presents the initial chloride concentration distribution in the Lower Yorktown–Eastover aquifer, which serves as the baseline condition for subsequent transport simulations. Fig. 10, 2080 map incorporates both a dry precipitation pattern (reduced recharge under a BCC SSP2-4.5 scenario) and a gradual SLR of 4 mm/yr imposed via a rising general-head boundary every decade. Although recent years suggest a slightly accelerated rate of up to 5 mm/year, a conservative rate of 4 mm/year was selected to align with the long-term trend and maintain consistency (NOAA,2024). The 2080 simulations indicate that chloride

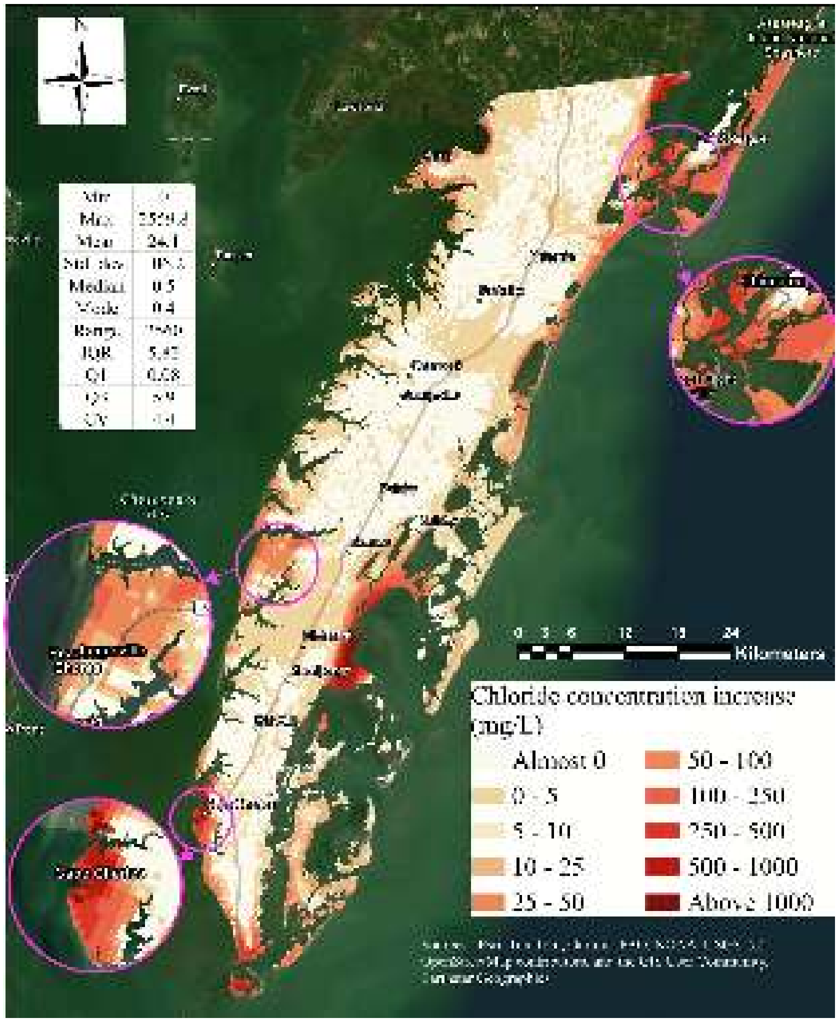

Fig. 10. Projected chloride concentration increase (mg/L) with statistics in the Lower Yorktown aquifer for 2080 compared to 2023 under combined drier GCMs-driven recharge (BCC-CSM2-MR) and SLR scenarios.

concentration increases are highly spatially heterogeneous and strongly localized to coastal margins and tidal creek networks under both SLR–only (See Fig. SF18 a) and combined SLR–drier scenarios (see Fig. 10). Across scenarios, median increases remain below 1 mg/L and interquartile ranges are small, while maximum values exceed 2500 mg/L, reflecting a pronounced right-skewed distribution dominated by a limited number of coastal and barrier-island cells. The large coefficients of variation (>4 for SLR-only and SLR + BCC) further confirm that mean values are driven by localized salinization hotspots rather than widespread inland impacts.

Under SLR-only conditions, elevated chloride increases are concentrated along low-lying shorelines, marshes, and barrier islands (e.g., Cape Charles and Chincoteague), consistent with density-driven intrusion and enhanced exchange with saline surface waters. The addition of drier climate forcing under the BCC intermediate scenario produces modest incremental changes relative to SLR alone, with a mean difference of approximately 2 mg/L (See Fig. SF18 b). This indicates that, in the drier future, reduced recharge limits inland propagation of salinity and constrains climate-driven effects primarily to areas already sensitive to SLR.

The difference map highlights that climate-induced modifications largely amplify chloride increases at existing coastal hotspots rather than creating large new inland zones of salinization. These results suggest that, by 2080, SLR remains the dominant control on chloride dynamics in the system, while climate-driven recharge changes play a secondary role. From a management perspective, this implies that adaptation efforts should prioritize low-elevation coastal communities and barrier environments for SWI monitoring, where even small changes in recharge can exacerbate salinity impacts under rising sea levels, while much of the inland aquifer remains comparatively resilient under drier climate projections.

4.6. Groundwater dynamics and management implications

The ESVA surficial aquifer exhibits topography-limited behavior in low-lying coastal and wetland settings, typical of low-relief coastal plains. In inland areas where the water table remains below land surface, consistent with MIKE SHE simulations in the Argentine Pampas (García et al., 2018), where low gradients and weakly developed channelized drainage promote strong vertical water-table responses, the ESVA water table across much of the peninsula varies primarily as a function of climate-driven recharge, with lateral discharge occurring largely through diffuse groundwater–surface-water exchange with wetlands, tidal creeks, and ultimately the coastal margins. This hydrogeologic setting helps explain why water-table elevations can increase under wetter recharge scenarios, while the net change in freshwater storage (or freshwater thickness) may remain modest.

Although the ensemble spread in total freshwater volume is modest (5.2% between the driest and wettest GCMs), this scalar metric masks much larger and management-relevant differences in groundwater heads and their spatial patterns. As shown in Fig. 8 (and Fig. SF13), inter-model ranges in surficial-aquifer head exceed 2 m along the peninsula's central areas, with a range of 0–3 m. These decimeter- to meter-scale differences directly influence the risk of waterlogging for shallow infrastructure in wetter decades and the required pumping lift and energy demand during drier decades, even when total freshwater storage remains constrained by the aquifer's topographic constraints. It is also important to note that the ESVA relies heavily on septic systems for wastewater treatment, making shallow groundwater behavior particularly relevant for infrastructure resilience and water quality.

Accordingly, we retain the multi-model climate ensemble not only to quantify uncertainty in net storage change but also to delineate zones of diverging head and depth projections and provide credible upper and lower bounds on future groundwater states, bounds that can be refined as new monitoring data become available.

Taken together, our results indicate a spatially differentiated response of the aquifer: recharge-driven water-table variability dominate inland, whereas compounded recharge variability and SLR control salinity intrusion and groundwater depth along the coast. These patterns suggest a scenario-based, adaptive, dual-track strategy for groundwater management: (i) managing uplands for both drought and waterlogging arising from recharge variability, and (ii) designing coastal defenses and monitoring networks that explicitly account for shallow water-table conditions and salinity intrusion driven by SLR and recharge fluctuations.

4.7. Study limitations and opportunities for future research

This study acknowledges some limitations, including the uncertainty in recharge projections due to the use of generalized GCMs and assumptions regarding future precipitation and temperature patterns. Specifically, we acknowledged the uncertainties found in rainfall datasets for the baseline period (2001–2014) provided by GCMs (see section 3.2). In short, in coastal regions such as the ESVA, where (1) rainfall gauge networks are sparse and (2) satellite-based rainfall products (e.g., IMERGF) exhibit retrieval errors (Derin et al., 2022) appear to challenge hydrological simulations, we recommend incorporating Soil Moisture (SM)-based rainfall datasets, such as the SM2RAIN (Soil Moisture to Rain) – ASCAT data, which uses the bottom-up approach, instead of the traditional top-down method, to derive rainfall data from SM, which might better represent the rainfall intensity (Do et al., 2024).

In addition, while the groundwater model provides reliable long-term hydrologic forecasts, its annual stress period limits its ability to capture short-term changes like monthly fluctuations. The study applies sea-level rise as a uniform, linear boundary increase of 4 mm/yr and retains the original land/sea cell configuration. This simplification omits (i) non-linear acceleration in SLR projections and (ii) dynamic conversion of low-lying terrestrial cells to marine boundary conditions. Both effects could amplify coastal-groundwater responses in later decades and should be explored in future simulations.

Exploring varying SLR rates, land surface inundation processes, and finder discretization, site-specific recharge and pumping data would enhance model accuracy. Further investigation into monthly groundwater variations and the effects of changing land use and water demand on recharge and withdrawal rates would provide more comprehensive insights. Lastly, integrating socio-economic factors into groundwater modeling could improve water resource management strategies and help develop more efficient and equitable mitigation approaches.

5. Conclusions

This study evaluated the projected impacts of climate model variability on groundwater resources in ESVA, with a focus on changes in recharge, water table elevations, and freshwater volume. Four CMIP6 models, BCC-CSM2-MR, CanESM5, MIROC6, and MRI-ESM2-0, were considered, drawn from the NASA NEX-GDDP archive to span wet through dry futures and capture model diversity. CMIP6 climate outputs (SSP2-4.5, SSP5-8.5) were downscaled and used to run SWAT to generate spatially and temporally distributed recharge; these fields were passed to SEAWAT to simulate variable density flow and salinity with coastal general head boundaries adjusted for SLR. Key findings include:

(1) Decadal recharge multipliers range from –35% (BCC-CSM2-MR) to +55% (CanESM5). That spread drives surficial-aquifer head changes of –1.6 m to +1.9 m, almost 8 times larger than the shift produced by SLR alone.
(2) Models' disagreement is not spatially uniform. The greatest uncertainty is inland, where heads respond directly to divergent recharge projections, while coastal zones are constrained by the shared sea-level boundary and low relief. Model-to-model head range exceeds 2 m along the upland ridge but falls below 0.25 m on barrier islands, where the common SLR boundary dominates. Accordingly, targeted monitoring should prioritize the high-variance ridge, installing nested piezometer clusters to track recharge-driven trends and reduce projection uncertainty.
(3) We found that fresh surficial groundwater volume swings 2.6%, in which by 2080, the driest pathway (BCC-CSM2-MR, SSP2-4.5) contracts freshwater storage −2.5% (−181 M m^3), whereas the wettest (CanESM5, SSP2-4.5) expands it +2.7% (+209 M m^3), enough water to meet 33 years of domestic demand for the current 46,000-resident Eastern Shore. Ensemble averages mask this ± 190 M m^3 risk window, showing only a +0.1% change.
(4) High-GHG (SSP5-8.5) scenarios show the greatest interquartile range around 2030, but this range narrows after 2060. In contrast, the intermediate scenario continues to widen, reaching a 5.2% spread in fresh surficial groundwater volume by 2080.
(5) Along barrier islands and tidal-creek shorelines, SLR is the dominant trigger on SWI along ESVA's low-lying perimeter, while the inland groundwater remains largely stable when recharge is held constant in the Lower Yorktown–Eastover confined aquifer. When SLR is combined with reduced recharge, salinization expands both inland and upward. In the Lower Yorktown–Eastover aquifer, the domain-mean chloride concentration increases from 22.7 mg/L under SLR-only (2080) to 24.1 mg/L under SLR + BCC Intermediate (2080). Multi-year droughts can further depress recharge, amplify salinization and heighten water-supply stress.

In summary, this analysis highlights the complex, spatially heterogeneous, and model-dependent nature of recharge variability impacts on groundwater in coastal aquifers. It underscores the urgency of integrating climate projections into groundwater resource management and calls for robust, adaptive strategies that accommodate uncertainty and account for recharge variability.

Declaration of Generative AI and AI-assisted technologies in the writing process

During the preparation of this work, the authors used Chat-GPT to improve readability. After using this tool/service, the authors reviewed and edited the content as needed and take full responsibility for the content of the publication.

Notice**

This manuscript has been co-authored by staff from UT-Battelle, LLC, under contract DE-AC05-00OR22725 with the US Department of Energy (DOE). The US government retains and the publisher, by accepting the article for publication acknowledges, that the US government retains a nonexclusive, paid-up, irrevocable, worldwide license to publish or reproduce the published form of this manuscript, or allow others to do so, for US government purposes. DOE will provide public access to these results of federally sponsored research in accordance with the DOE Public Access Plan (https://energy.gov/downloads/doe-public-acce

ss-plan).

CRediT authorship contribution statement

Farshad Hesamfar: Writing – review & editing, Writing – original draft, Visualization, Validation, Software, Resources, Methodology, Investigation, Formal analysis, Data curation, Conceptualization. **Sergio A. Barbosa:** Writing – review & editing, Writing – original draft, Visualization, Validation, Software, Methodology, Investigation, Formal analysis, Data curation, Conceptualization. **Thanh-Nhan-Duc Tran:** Writing – review & editing, Writing – original draft, Visualization, Validation, Software, Resources, Methodology, Formal analysis, Data curation. **Teresa Culver:** Writing – review & editing, Supervision, Methodology, Funding acquisition. **Lawrence Band:** Writing – review & editing, Supervision, Funding acquisition. **Venkataraman Lakshmi:** Writing – review & editing, Supervision, Funding acquisition.

Declaration of competing interest

The authors declare that they have no known competing financial interests or personal relationships that could have appeared to influence the work reported in this paper.

Acknowledgements

This work was supported by the National Science Foundation, Award No. **2053013** (Focused CoPe: Building Capacity for Adaptation in Rural Coastal Communities). S. Barbosa acknowledges support from the University of Virginia's Environmental Institute and from the U.S. Department of Energy, Office of Science, Biological and Environmental Research program, through the Southeast Texas Urban Integrated Field Laboratory project.

Appendix A. Supplementary data

Supplementary data to this article can be found online at https://doi.org/10.1016/j.jhydrol.2026.135003.

Data availability

Data will be made available on request.

References

Akhtar, J., Sana, A., Tauseef, S.M., Tanaka, H., 2022. Numerical modeling of seawater intrusion in Wadi Al-Jizi Coastal Aquifer in the Sultanate of Oman. Hydrology 9 (12), 211. https://doi.org/10.3390/hydrology9120211.

Aladejana, J.A., Kalin, R.M., Sentenac, P., Hassan, I., 2020. Assessing the impact of climate change on groundwater quality of the shallow coastal aquifer of eastern dahomey basin, southwestern Nigeria. Water 12 (1), 224. https://doi.org/10.3390/w12010224.

Almazroui, M., Ashfaq, M., Islam, M.N., Rashid, I.U., Kamil, S., Abid, M.A., Sylla, M.B., 2021. Assessment of CMIP6 performance and projected temperature and precipitation changes over South America. Earth Systems and Environment 5 (2), 155–183. https://doi.org/10.1007/s41748-021-00233-6.

Andrews, E., King, A., Kraus, J., West, A., 2019. Flooding and Sea Level Rise on the Eastern Shore: Frequently Asked Questions.

Arnold, J.G., Moriasi, D.N., Gassman, P.W., Abbaspour, K.C., White, M.J., Srinivasan, R., Jha, M.K., 2012. SWAT: Model use, calibration, and validation. Transactions of the ASABE 55 (4), 1491–1508.

Aryal, A., Kumar, B., Lakshmi, V., 2023. Evaluation of satellite-derived precipitation products for streamflow simulation of a mountainous Himalayan watershed: a study of Myagdi Khola in Kali Gandaki basin, Nepal. Remote Sensing 15 (19), 4762. https://doi.org/10.3390/rs15194762.

Ashofteh, P., Jalili, S., Loáiciga, H.A., 2025. Assessment of climate change uncertainty effects on groundwater level prediction using Bayesian analysis, Theor. Appl. Climatol. https://doi.org/10.1007/s00704-024-05308-8.

Asoka, A., Gleeson, T., Wada, Y., Mishra, V., 2017. Relative contribution of monsoon precipitation and pumping to changes in groundwater storage in India. Nat. Geosci. 10 (2), 109–117. https://doi.org/10.1038/ngeo2869.

Barnard, P.L., Befus, K.M., Danielson, J.J., Engelstad, A.C., Erikson, L.H., Foxgrover, A. C., Hayden, M.K., Hoover, D.J., Leijnse, T.W.B., Massey, C., McCall, R., Nadal-Caraballo, N.C., Nederhoff, K., O'Neill, A.C., Parker, K.A., Shirzaei, M., Ohenhen, L. O., Swarzenski, P.W., Thomas, J.A., Jones, J.L., 2025. Projections of multiple climate-related coastal hazards for the US Southeast Atlantic. Nat. Clim. Chang. 15 (1), 101–109. https://doi.org/10.1038/s41558-024-02180-2.

Chang, S.W., Clement, T.P., Simpson, M.J., Lee, K.-K., 2011. Does sea-level rise have an impact on saltwater intrusion? Adv. Water Resour. 34 (10), 1283–1291. https://doi.org/10.1016/j.advwatres.2011.06.006.

Chen, C., Gan, R., Feng, D., Yang, F., Zuo, Q., 2022. Quantifying the contribution of SWAT modeling and CMIP6 inputting to streamflow prediction uncertainty under climate change. J. Clean. Prod. 364, 132675. https://doi.org/10.1016/j.jclepro.2022.132675.

Chesapeake Bay Foundation, 2018. Chesapeake Bay Foundation. https://www.cbf.org/index.html.

Chun, J., Lim, C., Kim, D., Kim, J., 2018. Assessing impacts of climate change and sea-level rise on seawater intrusion in a Coastal Aquifer. Water 10 (4), 357. https://doi.org/10.3390/w10040357.

Cianflone, G., Vespasiano, G., Tolomei, C., De Rosa, R., Dominici, R., Apollaro, C., Walraevens, K., Polemio, M., 2022. Different ground subsidence contributions revealed by integrated discussion of Sentinel-1 datasets, well discharge, stratigraphical and geomorphological data: the case of the Gioia Tauro Coastal Plain (Southern Italy). Sustainability 14 (5), 2926. https://doi.org/10.3390/su14052926.

Claggett, P. R., McDonald, S. M., O'Neil-Dunne, J., MacFaden, S., Walker, K., Guinn, S., Ahmed, L., Buford, E., Kurtz, E., McCabe, P., Pickford, J. A., Royar, A., Schulze, K., 2025, Chesapeake Bay Land Use/Land Cover (LULC) Database 2024 Edition: U.S. Geological Survey data release, https://doi.org/10.5066/P14BEBRC.

Dao, P.U., Heuzard, A.G., Le, T.X.H., Zhao, J., Yin, R., Shang, C., Fan, C., 2024. The impacts of climate change on groundwater quality: a review. Sci. Total Environ. 912, 169241. https://doi.org/10.1016/j.scitotenv.2023.169241.

Davamani, V., John, J.E., Poornachandhra, C., Gopalakrishnan, B., Arulmani, S., Parameswari, E., Santhosh, A., Srinivasulu, A., Lal, A., Naidu, R., 2024. A critical review of climate change impacts on groundwater resources: a focus on the current status, future possibilities, and role of simulation models. Atmos 15 (1), 122. https://doi.org/10.3390/atmos15010122.

de Graaf, I.E.M., van Beek, R.L.P.H., Gleeson, T., Moosdorf, N., Schmitz, O., Sutanudjaja, E.H., Bierkens, M.F.P., 2017. A global-scale two-layer transient groundwater model: development and application to groundwater depletion. Adv. Water Resour. 102, 53–67. https://doi.org/10.1016/j.advwatres.2017.01.011.

Derin, Y., Kirstetter, P.E., Brauer, N., Gourley, J.J., Wang, J., 2022. Evaluation of IMERG satellite precipitation over the land–coast–ocean continuum. Part II: Quantification. Journal of Hydrometeorology 23 (8), 1297–1314. https://doi.org/10.1175/JHM-D-21-0234.1.

Dile, Y., Srinivasan, R., George, C., 2016. QGIS Interface for SWAT (QSWAT). Version, 1, 25. https://swat.tamu.edu/media/116371/qswat-manual_v19.pdf.

Do, S.K., Tran, T.N.D., Le, M.H., Bolten, J., Lakshmi, V., 2024. A novel validation of satellite soil moisture using SM2RAIN-derived rainfall estimates. Frontiers in Remote Sensing 5, 1474088. https://doi.org/10.3389/frsen.2024.1474088.

EL Hamidi, M., Larabi, A., Faouzi, M., 2021. Numerical modeling of saltwater intrusion in the Rmel-Oulad Ogbane Coastal Aquifer (Larache, Morocco) in the climate change and sea-level rise context (2040). Water 13 (16), 2167. https://doi.org/10.3390/w13162167.

EPA, 2025. Sole Source Aquifers for Drinking Water | US EPA. https://www.epa.gov/dwssa.

Fidelibus, M. D., Balacco, G., Alfio, M. R., Arfaoui, M., Bassukas, D., Güler, C., Hamzaoui-Azaza, F., Külls, C., Panagopoulos, A., Parisi, A., Sachsamanoglou, E., Tziritis, E., 2025. A chloride threshold to identify the onset of seawater/saltwater intrusion and a novel categorization of groundwater in coastal aquifers. https://doi.org/10.1016/j.jhydrol.2025.132775.

García, P.E., et al., 2018. Land use as possible strategy for managing water table depth in flat basins with shallow groundwater. Int. J. River Basin Manage. 16 (1), 79–92. https://doi.org/10.1080/15715124.2017.1378223.

Guo, W., Langevin, C.D., 2002. User's guide to SEAWAT—a computer program for simulation of three-dimensional variable-density ground-water flow. U.S. Geol. Surv. Open File Rep. 01 (434), 77.

Gupta, H.V., Kling, H., Yilmaz, K.K., Martinez, G.F., 2009. Decomposition of the mean squared error and NSE performance criteria: Implications for improving hydrological modelling. J. Hydrol. 377 (1–2), 80–91. https://doi.org/10.1016/j.jhydrol.2009.08.003.

Hagagg, K.H., 2018. Numerical modeling of seawater intrusion in karstic aquifer, Northwestern Coast of Egypt. Model. Earth Syst. Environ. 5 (2), 1–11. https://doi.org/10.1007/s40808-018-0549-3.

Han, D., Currell, M.J., 2022. Review of drivers and threats to coastal groundwater quality in China. Sci. Total Environ. 806 (Pt 4), 150913. https://doi.org/10.1016/j.scitotenv.2021.150913.

Herrera-García, G., Ezquerro, P., Tomás, R., Béjar-Pizarro, M., López-Vinielles, J., Rossi, M., Mateos, R.M., Carreón-Freyre, D., Lambert, J., Teatini, P., Cabral-Cano, E., Erkens, G., Galloway, D., Hung, W.-C., Kakar, N., Sneed, M., Tosi, L., Wang, H., Ye, S., 2021. Mapping the global threat of land subsidence. Science 371 (6524), 34–36. https://doi.org/10.1126/science.abb8549.

Hesamfar, F., Ketabchi, H., Ebadi, T., 2023a. Simulation-based multi-objective optimization framework for sustainable management of coastal aquifers in semi-arid regions. J. Environ. Manage. 338, 117785. https://doi.org/10.1016/j.jenvman.2023.117785.

Hesamfar, F., Ketabchi, H., Ebadi, T., 2023b. Multi-dimensional management framework on fresh groundwater lens of Kish Island in the Persian Gulf, Iran. J. Environ. Manage. 347, 119032. https://doi.org/10.1016/j.jenvman.2023.119032.

Hou, A.Y., Kakar, R.K., Neeck, S., Azarbarzin, A.A., Kummerow, C.D., Kojima, M., Iguchi, T., 2014. The global precipitation measurement mission. Bull. Am. Meteorol. Soc. 95 (5), 701–722. https://doi.org/10.1175/BAMS-D-13-00164.1.

IGRAC, 2024. IGRAC Strategy 2024-2027: For a Sustainable & Equitable Groundwater Future | International Groundwater Resources Assessment Centre. https://www.un-igrac.org/resource/igrac-strategy-2024-2027-sustainable-equitable-groundwater-future.

Ketabchi, H., Mahmoodzadeh, D., Ataie-Ashtiani, B., Simmons, C.T., 2016 Apr. Sea-level rise impacts on seawater intrusion in coastal aquifers: Review and integration. J. Hydrol. (Amst). 535, 235–255. https://doi.org/10.1016/j.jhydrol.2016.01.083.

Khalid, K., Ali, M.F., Abd Rahman, N.F., Mispan, M.R., Haron, S.H., Othman, Z., Bachok, M.F., 2016. Sensitivity analysis in watershed model using SUFI-2 algorithm. Procedia Eng. 162, 441–447. https://doi.org/10.1016/j.proeng.2016.11.086.

Lam, Q. D., Meon, G., Ptsch, M., 2021. Coupled modelling approach to assess effects of climate change on a coastal groundwater system. Elsevier BV. https://doi.org/10.1016/j.gsd.2021.100633.

Langevin, C.D., Shoemaker, W.B., Guo, W., 2003. MODFLOW-2000, the U.S. Geological Survey Modular Ground-Water Model-Documentation of the SEAWAT-2000 Version with the Variable-Density Flow Process (VDF) and the Integrated MT3DMS Transport Process (IMT). USGS Publications Warehouse 03 (426), 43.

Le, M.H., Zhang, R., Nguyen, B.Q., Bolten, J.D., Lakshmi, V., 2023. Robustness of gridded precipitation products for Vietnam basins using the comprehensive assessment framework of rainfall. Atmos. Res. 293, 106923. https://doi.org/10.1016/j.atmosres.2023.106923.

Lehner, B., Grill, G., 2013. Global river hydrography and network routing: baseline data and new approaches to study the world's large river systems. Hydrol. Process. 27 (15), 2171–2186. https://doi.org/10.1002/hyp.9740.

Marshall, A., Grubert, E., Warix, S., 2025. Temperature overshoot would have lasting impacts on hydrology and water resources. Water Resour. Res. 61 (1). https://doi.org/10.1029/2024WR037950.

Maurer, E.P., Hidalgo, H.G., 2008. Utility of daily vs. monthly large-scale climate data: an intercomparison of two statistical downscaling methods. Hydrol. Earth Syst. Sci. 12 (2), 551–563. https://doi.org/10.5194/hess-12-551-2008.

Michael, H.A., Russoniello, C.J., Byron, L.A., 2013. Global assessment of vulnerability to sea-level rise in topography-limited and recharge-limited coastal groundwater systems. Water Resour. Res. 49 (4), 2228–2240. https://doi.org/10.1002/wrcr.20213.

Moriasi, D.N., Gitau, M.W., Pai, N., Daggupati, P., 2015. Hydrologic and water quality models: performance measures and evaluation criteria. Trans. ASABE 58 (6), 1763–1785. https://doi.org/10.13031/trans.58.10715.

Nash, J.E., Sutcliffe, J.V., 1970. River flow forecasting through conceptual models part I — a discussion of principles. J. Hydrol. 10 (3), 282–290. https://doi.org/10.1016/0022-1694(70)90255-6.

NEX-GDDP-CMIP6, 2025. NASA Earth Exchange Global Daily Downscaled Projections (NEX-GDDP-CMIP6) | NASA Center for Climate Simulation. https://www.nccs.nasa.gov/services/data-collections/land-based-products/nex-gddp-cmip6.

Nguyen, T.V., Dietrich, J., Dang, T.D., Tran, D.A., Van Doan, B., Sarrazin, F.J., Srinivasan, R., 2022. An interactive graphical interface tool for parameter calibration, sensitivity analysis, uncertainty analysis, and visualization for the Soil and Water Assessment Tool. Environ. Model. Software 156, 105497. https://doi.org/10.1016/j.envsoft.2022.105497.

Nguyen, B.Q., Van Binh, D., Tran, T.-N.-D., Kantoush, S.A., Sumi, T., 2024. Response of streamflow and sediment variability to cascade dam development and climate change in the Sai Gon Dong Nai River basin. Clim. Dyn. 62 (8), 7997–8017. https://doi.org/10.1007/s00382-024-07319-7.

NOAA, 2024. Sea level trends – Kiptopeke, Virginia (Station #8632200). National Oceanic and Atmospheric Administration, National Ocean Service, Center for Operational Oceanographic Products and Services (CO-OPS). Retrieved from https://tidesandcurrents.noaa.gov/sltrends/sltrends_station.shtml?id=8632200.

Nowroozi, A.A., Horrocks, S.B., Henderson, P., 1999. Saltwater intrusion into the freshwater aquifer in the eastern shore of Virginia: a reconnaissance electrical resistivity survey. J. Appl. Geophys. 42 (1), 1–22. https://doi.org/10.1016/S0926-9851(99)00004-X.

Oude Essink, G.H.P., van Baaren, E.S., de Louw, P.G.B., 2010. Effects of climate change on coastal groundwater systems: a modeling study in the Netherlands. Water Resour. Res. 46 (10). https://doi.org/10.1029/2009WR008719.

Park, T., Hashimoto, H., Wang, W., Thrasher, B., Michaelis, A.R., Lee, T., Brosnan, I.G., Nemani, R.R., 2023. What does global land climate look like at 2°C warming? Earth's. Future 11 (5). https://doi.org/10.1029/2022EF003330.

Payne, D.F., 2010. Effects of climate change on saltwater intrusion at Hilton HeadIsland, SC. U.S.A. SWIM21 – 21st Salt Water Intrusion Meeting.

Peng, S., Wang, C., Li, Z., Mihara, K., Kuramochi, K., Toma, Y., Hatano, R., 2023. Climate change multi-model projections in CMIP6 scenarios in Central Hokkaido, Japan. Sci. Rep. 13 (1), 230. https://doi.org/10.1038/s41598-022-27357-7.

Poeter, E.P., Hill, M.C., 1999. UCODE, a computer code for universal inverse modeling. Elsevier BV. https://doi.org/10.1016/s0098-3004(98)00149-6.

Polemio, M., 2016. Monitoring and management of karstic coastal groundwater in a changing environment (southern italy): a review of a regional experience. Water 8 (4), 148. https://doi.org/10.3390/w8040148.

Rahimi, R., Tavakol-Davani, H., Graves, C., Gomez, A., Fazel Valipour, M., 2020. Compound inundation impacts of coastal climate change: sea-level rise, groundwater rise, and coastal precipitation. Water 12 (10), 2776. https://doi.org/10.3390/w12102776.

Ranjan, P., Kazama, S., Sawamoto, M., 2006. Effects of climate change on coastal fresh groundwater resources. Glob. Environ. Chang. 16 (4), 388–399. https://doi.org/10.1016/j.gloenvcha.2006.03.006.

Reinecke, R., Müller Schmied, H., Trautmann, T., Andersen, L.S., Burek, P., Flörke, M., Gosling, S.N., Grillakis, M., Hanasaki, N., Koutroulis, A., Pokhrel, Y., Thiery, W., Wada, Y., Yusuke, S., Döll, P., 2021. Uncertainty of simulated groundwater recharge at different global warming levels: a global-scale multi-model ensemble study. Hydrol. Earth Syst. Sci. 25 (2), 787–810. https://doi.org/10.5194/hess-25-787-2021.

Richardson, D.L., 1994. Hydrogeology and analysis of the ground-water-flow system of the eastern shore. Virginia. https://doi.org/10.3133/wsp2401.

Richardson, C.M., Davis, K.L., Ruiz-González, C., Guimond, J.A., Michael, H.A., Paldor, A., Moosdorf, N., Paytan, A., 2024. The impacts of climate change on coastal groundwater. Nat. Rev. Earth Environ. 5 (2), 100–119. https://doi.org/10.1038/s43017-023-00500-2.

Russo, T.A., Lall, U., 2017. Depletion and response of deep groundwater to climate-induced pumping variability. Nat. Geosci. 10 (2), 105–108. https://doi.org/10.1038/ngeo2883.

Saber, M., Sumi, T., 2023. Response of hydrological to anthropogenic activities in a tropical basin. In Proceedings of the 40th IAHR World Congress, Vienna, Austria (pp. 21-25). https://doi.org/10.3850/978-90-833476-1-5_iahr40wc-p1339-cd.

Saeedi, M., Sharafati, A., Brocca, L., Tavakol, A., 2022. Estimating rainfall depth from satellite-based soil moisture data: a new algorithm by integrating SM2RAIN and the analytical net water flux models. J. Hydrol. 610, 127868. https://doi.org/10.1016/j.jhydrol.2022.127868.

Sanford, W.E., Pope, J.P., 2007. A simulation of groundwater discharge and nitrate delivery to chesapeake bay from the lowermost Delmarva peninsula, USA.

Sanford, W.E., Pope, J.P., 2010. Current challenges using models to forecast seawater intrusion: lessons from the Eastern Shore of Virginia, USA. Hydrgeol. J. 18 (1), 73–93. https://doi.org/10.1007/s10040-009-0513-4.

Sanford, W.E., Pope, J.P., Nelms, D.L., 2009. Simulation of Groundwater-Level and Salinity Changes in the Eastern Shore, Virginia. Scientific Investigations Report.

Sathish, S., Chanu, S., Sadath, R., Elango, L., 2022. Impacts of regional climate model projected rainfall, sea level rise, and urbanization on a coastal aquifer. Environ. Sci. Pollut. Res. Int. 29 (22), 33305–33322. https://doi.org/10.1007/s11356-021-18213-8.

Scibek, J., Allen, D.M., 2006. Modeled impacts of predicted climate change on recharge and groundwater levels. Am. Geophys. Union (AGU). https://doi.org/10.1029/2005wr004742.

Scibek, J., Allen, D.M., Cannon, A.J., Whitfield, P.H., 2007. Groundwater–surface water interaction under scenarios of climate change using a high-resolution transient groundwater model. Elsevier BV. https://doi.org/10.1016/j.jhydrol.2006.08.005.

Sherif, M.M., Singh, V.P., 1999. Effect of climate change on sea water intrusion in coastal aquifers. Hydrol. Process. 13 (8), 1277–1287. https://doi.org/10.1002/(SICI)1099-1085(19990615)13:8<1277::AID-HYP765>3.0.CO;2-W.

Sithara, S., Pramada, S.K., Thampi, S.G., 2020. Impact of projected climate change on seawater intrusion on a regional coastal aquifer. J. Earth Syst. Sci. 129 (1), 218. https://doi.org/10.1007/s12040-020-01485-y.

Sivarajan, N.A., Mishra, A.K., Rafiq, M., Nagraju, V., Chandra, S., 2019. Examining climate change impact on the variability of ground water level: a case study of Ahmednagar district, India. J. Earth Syst. Sci 128 (5), 122. https://doi.org/10.1007/s12040-019-1172-z.

Smith, C., 2015. Eastern Shore Master Gardeners Overview of Ground Water on the Eastern Shore. Accomack-Northampton Planning District Commission. https://www.esvaplan.org/wp-content/uploads/2024/05/Overview-of-Ground-Water-on-the-Eastern-Shore-1.pdf.

Speiran, G.K., 1996. Geohydrology and geochemistry near coastal ground-water-discharge areas of the Eastern Shore, Virginia. U.S Geological Survey Water-Supply Paper 2479, 73 p.

Srivastava, A., Grotjahn, R., Ullrich, P.A., 2020. Evaluation of historical CMIP6 model simulations of extreme precipitation over contiguous US regions. Weather and Climate Extremes 29, 100268. https://doi.org/10.1016/j.wace.2020.100268.

Tam, V.T., Batelaan, O., Beyen, I., 2016. Impact assessment of climate change on a coastal groundwater system, Central Vietnam. Environ. Earth Sci. 75 (10), 908. https://doi.org/10.1007/s12665-016-5718-y.

Tapas, M.R., Etheridge, R., Tran, T.-N.-D., Finlay, C.G., Peralta, A.L., Bell, N., Xu, Y., Lakshmi, V., 2024. A methodological framework for assessing sea level rise impacts on nitrate loading in coastal agricultural watersheds using SWAT+: a case study of the Tar-Pamlico River basin, North Carolina, USA. Sci. Total Environ. 951, 175523. https://doi.org/10.1016/j.scitotenv.2024.175523.

Tarboton, D.G., 2011. TauDEM 5.0. Watershed delineation using TauDEM. A tutorial for using TauDEM to delineate a single watershed. https://hydrology.usu.edu/taudem/taudem5/TauDEM5DelineatingASingleWatershed.pdf.

Thrasher, B., Wang, W., Michaelis, A., Melton, F., Lee, T., Nemani, R., 2022. NASA global daily downscaled projections, CMIP6. Sci. Data 9 (1), 262. https://doi.org/10.1038/s41597-022-01393-4.

Tiwari, S., Saviano, S., Polemio, M., 2024. Modelling approach integrating climate projections for coastal groundwater management. Sci. Total Environ. 949, 175216. https://doi.org/10.1016/j.scitotenv.2024.175216.

Tran, T.-N.-D., Lakshmi, V., 2024. Enhancing human resilience against climate change: Assessment of hydroclimatic extremes and sea level rise impacts on the Eastern Shore of Virginia, United States. Sci. Total Environ. 947, 174289. https://doi.org/10.1016/j.scitotenv.2024.174289.

Tran, T.-N.-D., Nguyen, B.Q., Grodzka-Łukaszewska, M., Sinicyn, G., Lakshmi, V., 2023. The role of reservoirs under the impacts of climate change on the Srepok River basin, Central Highlands of Vietnam. Front. Environ. Sci. 11. https://doi.org/10.3389/fenvs.2023.1304845.

Tran, T.-N.-D., Do, S.K., Nguyen, B.Q., Tran, V.N., Grodzka-Łukaszewska, M., Sinicyn, G., Lakshmi, V., 2024a. Investigating the future flood and drought shifts in the

transboundary Srepok River basin using CMIP6 projections. IEEE J. Sel. Top. Appl. Earth Obs. Remote Sens. 1–16. https://doi.org/10.1109/JSTARS.2024.3380514.
Tran, T.-N.-D., Tapas, M.R., Do, S.K., Etheridge, R., Lakshmi, V., 2024b. Investigating the impacts of climate change on hydroclimatic extremes in the Tar-Pamlico River basin, North Carolina. J. Environ. Manage. 363, 121375. https://doi.org/10.1016/j.jenvman.2024.121375.
U.S. Census Bureau, 2021. 2020 Decennial Census: Population and Housing for Virginia. U.S. Department of Commerce. https://data.census.gov/.
U.S. Fish & Wildlife Service, 2018. Eastern Shore of Virginia National Wildlife Refuge | U.S. Fish & Wildlife Service. https://www.fws.gov/refuge/eastern-shore-virginia.
U.S. Geological Survey. (n.d.) Virginia Eastern Shore groundwater. U.S. Department of the Interior. https://www.usgs.gov/centers/virginia-and-west-virginia-water-science-center/science/virginia-eastern-shore-groundwater.
Vandenbohede, A., Lebbe, L., 2010. Impact of climate change on the phreatic aquifer of the western Belgian coastal plain. SWIM21 – 21 St Salt Water Intrusion Meeting.
van der Knaap, Y.A.M., de Graaf, M., van Ek, R., Witte, J.-P.-M., Aerts, R., Bierkens, M.F.P., van Bodegom, P.M., 2015. Potential impacts of groundwater conservation measures on catchment-wide vegetation patterns in a future climate. Landsc. Ecol. 30 (5), 855–869. https://doi.org/10.1007/s10980-014-0142-8.
van Engelenburg, J., Hueting, R., Rijpkema, S., Teuling, A.J., Uijlenhoet, R., Ludwig, F., 2017. Impact of changes in groundwater extractions and climate change on groundwater-dependent ecosystems in a complex hydrogeological setting. Water Resour. Manag. 32 (1), 1–14. https://doi.org/10.1007/s11269-017-1808-1.
Vespasiano, G., Cianflone, G., Romanazzi, A., Apollaro, C., Dominici, R., Polemio, M., De Rosa, R., 2019. A multidisciplinary approach for sustainable management of a complex coastal plain: the case of Sibari Plain (Southern Italy). Mar. Pet. Geol. 109, 740–759. https://doi.org/10.1016/j.marpetgeo.2019.06.031.
Virginia Department of Environmental Quality (VADEQ), 2024. Virginia State Water Resources Plan. Virginia Eastern Shore Model (VAHydroGW-ES) 2023-2024 Annual simulation of potentiometric groundwater surface elevations of reported and total permitted use. Office of Water Supply. https://www.deq.virginia.gov/our-programs/water/water-quantity/water-supply-planning/virginia-water-resources-plan.
Vu, C.H., Nguyen, B.Q., Tran, T.-N.-D., Vo, D.N., Arshad, A., 2024. Climate change-driven hydrological shifts in the Kon-Ha Thanh River Basin. Water 16 (23), 3389. https://doi.org/10.3390/w16233389.
Wang, T., Tu, X., Singh, V.P., Chen, X., Lin, K., 2021. Global data assessment and analysis of drought characteristics based on CMIP6. J. Hydrol. 596, 126091. https://doi.org/10.1016/j.jhydrol.2021.126091.
Werner, A.D., Simmons, C.T., 2009. Impact of sea-level rise on sea water intrusion in coastal aquifers. Groundwater 47 (2), 197–204. https://doi.org/10.1111/j.1745-6584.2008.00535.x.
Werner, A.D., Ward, J.D., Morgan, L.K., Simmons, C.T., Robinson, N.I., Teubner, M.D., 2012. Vulnerability indicators of sea water intrusion. Groundwater 50 (1), 48–58. https://doi.org/10.1111/j.1745-6584.2011.00817.x.
Xu, X., Yun, X., Tang, Q., Cui, H., Wang, J., Zhang, L., Chen, D., 2023. Projected seasonal changes in future rainfall erosivity over the Lancang-Mekong River basin under the CMIP6 scenarios. J. Hydrol. 620, 129444. https://doi.org/10.1016/j.jhydrol.2023.129444.
Yamazaki, D., Ikeshima, D., Sosa, J., Bates, P.D., Allen, G.H., Pavelsky, T.M., 2019. MERIT Hydro: a high-resolution global hydrography map based on latest topography dataset. Water Resour. Res. 55 (6), 5053–5073. https://doi.org/10.1029/2019WR024873.
Yang, H., Yang, T., Yang, F., Yang, X., 2023. Assessment of groundwater salinization impact in coastal aquifers based on the shared socioeconomic pathways: an integrated modeling approach. Environ. Res. 234, 116618. https://doi.org/10.1016/j.envres.2023.116618.
Zhou, Y., Zwahlen, F., Wang, Y., Li, Y., 2010. Impact of climate change on irrigation requirements in terms of groundwater resources. Hydrgeol. J. 18 (7), 1571–1582. https://doi.org/10.1007/s10040-010-0627-8.